Frequency response analysis for reset control systems

Application to predict precision of motion systems

Zhang, Xinxin; Kaczmarek, Marcin B.; HosseinNia, S. Hassan

DOI
10.1016/j.conengprac.2024.106063

Publication date
2024

Document Version
Final published version

Published in
Control Engineering Practice

Control Engineering Practice 152 (2024) 106063

Contents lists available at ScienceDirect

Control Engineering Practice

journal homepage: www.elsevier.com/locate/conengprac

Frequency response analysis for reset control systems: Application to predict precision of motion systems

Xinxin Zhang, Marcin B. Kaczmarek, S. Hassan HosseinNia *

Department of Precision and Microsystems Engineering (PME), Delft University of Technology, Mekelweg 2, Delft, 2628CD, The Netherlands

ARTICLE INFO

MSC:
93C80
93C10
70Q05

Keywords:
Reset control system
Frequency response analysis
Steady state
Closed-loop
Higher-order sinusoidal-input describing functions
Precision motion

ABSTRACT

The frequency response analysis describes the steady-state responses of a system to sinusoidal inputs at different frequencies, providing control engineers with an effective tool for designing control systems in the frequency domain. However, conducting this analysis for closed-loop reset systems is challenging due to system nonlinearity. This paper addresses this challenge through two key contributions. First, it introduces novel analysis methods for both open-loop and closed-loop reset control systems at steady states. These methods decompose the frequency responses of reset systems into base-linear and nonlinear components. Second, building upon this analysis, the paper develops closed-loop higher-order sinusoidal-input describing functions for reset control systems at steady states. These functions facilitate the analysis of frequency-domain properties, establish a connection between open-loop and closed-loop analysis. The accuracy and effectiveness of the proposed methods are successfully validated through simulations and experiments conducted on a reset Proportional–Integral–Derivative (PID) controlled precision motion system.

1. Introduction

This paper aims to develop a method for analyzing the frequency response of reset control systems. The development of the reset element starts from the Clegg integrator (CI), introduced in 1958 (Clegg, 1958). The CI is a linear integrator encapsulating with a reset mechanism, which enables the output of the CI to be reset to zero whenever its input crosses zero. Through the Describing Function (DF) analysis, the CI demonstrates the same gain-frequency characteristics as a linear integrator but exhibits a significant phase lead of 51.9°. This phase-frequency characteristic highlights the ability of the reset element to overcome the Bode gain-phase restriction in linear controllers (Chen et al., 2018). Numerous other reset elements have been developed, including the First-order Reset Element (FORE) (Horowitz & Rosenbaum, 1975; Krishnan & Horowitz, 1974), the Second-order Reset Element (SORE) (Hazeleger et al., 2016), partial reset techniques (Beker et al., 2004), Proportional-Integral (PI) + CI (Baños & Vidal, 2007), reset control systems with reset bands (Baños et al., 2011), Fractional-order Reset Element (FrORE) (Saikumar & HosseinNia, 2017; Weise et al., 2019, 2020), and Constant in gain Lead in phase (CgLp) (Saikumar et al., 2019). Leveraging their gain-phase advantages, reset control elements have demonstrated improvements in steady-state and transient performance compared to linear controllers, including enhanced disturbance rejection, improved tracking, and reduced overshoot, see Deenen et al. (2021), Heertjes et al. (2016), Karbasizadeh and HosseinNia (2022), Saikumar et al. (2019), Zhao et al. (2020, 2019), Zhao and Wang (2015, 2016).

Frequency response analysis is a method used to assess the magnitude and phase properties of a control system by analyzing its steady-state responses to sinusoidal inputs across various frequencies (Tian & Gao, 2007). Engineers can shape and tune the performance of closed-loop systems based on their open-loop analysis, a technique referred to as loop shaping (Ogata, 2010; Van Loon et al., 2017). The frequency-domain-based loop shaping approach has proven effective for designing linear control systems, including PID controllers, in industries (Deenen et al., 2017; Saikumar et al., 2021, 2019). Reset controllers are seamlessly integrated into the classical PID framework, thus attracting interest for their potential applications across various industries (Beerens et al., 2021). However, the lack of effective frequency-domain analysis tools tailored for reset control systems has hindered their widespread adoption in industries.

The frequency response analysis includes both open-loop and closed-loop analysis. For open-loop reset controllers, the DF (Guo et al., 2009) was first employed to analyze their frequency response, but it falls short in capturing the complete dynamics of reset control systems as it only analyzes the first harmonic of the outputs. The Higher-Order Sinusoidal Input Describing Function (HOSIDF) (Saikumar et al., 2021), which accounts for higher-order harmonics, proves to be an effective method for analyzing open-loop reset control systems.

* Corresponding author.
E-mail addresses: X.Zhang-15@tudelft.nl (X. Zhang), MBKaczmarek@tudelft.nl (M.B. Kaczmarek), S.H.HosseinNiaKani@tudelft.nl (S.H. HosseinNia).

https://doi.org/10.1016/j.conengprac.2024.106063
Received 9 April 2024; Received in revised form 18 August 2024; Accepted 19 August 2024
Available online 2 September 2024

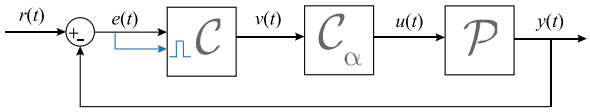

Fig. 1. The block diagram of the reset control system, where $r(t)$, $e(t)$, $v(t)$, $u(t)$, and $y(t)$ denote the reference input signal, the error signal, the reset output signal, the control input signal, and the output signal, respectively. The blue lines indicate the reset-triggered actions, with $e(t)$ serving as the reset-triggered signal in this system. (For interpretation of the references to color in this figure legend, the reader is referred to the web version of this article.)

However, in closed-loop reset control systems, the existence of high-order harmonics in the output signals leads to the generation of higher-order sub-harmonics through the feedback loop, presenting challenges for frequency response analysis. Existing tools for analyzing closed-loop reset control systems, such as pseudo-sensitivity functions in Dastjerdi et al. (2022), primarily rely on time-domain responses analysis approaches and lack a direct connection between open-loop and closed-loop analysis of reset control systems. The current frequency-domain-based analysis method for reset control systems in Saikumar et al. (2021) lacks precision as it overlooks certain higher-order harmonics in the closed-loop outputs.

The lack of precise frequency response analysis methods for closed-loop reset systems and the disconnect between open-loop and closed-loop analysis in reset systems motivates this research. The objective of this research is to develop new frequency response analysis methods for both open-loop and closed-loop reset control systems with sinusoidal inputs. These methods aim to (1) enable more accurate frequency-domain analysis of steady-state closed-loop reset control systems by rectifying the inaccuracies present in previous approaches, and (2) establish a reliable connection between the frequency-domain analysis of open-loop and closed-loop reset control systems.

The structure of the study is organized as follows. Section 2 provides definitions, discusses existing frequency response analysis methods for reset control systems, and states the research problems. The main contributions are detailed in Section 3 (for the open-loop reset system) and Section 4 (for the closed-loop reset system), including:

1. Theorem 1 presents a new pulse-based approach for analyzing open-loop reset systems. This method decomposes the steady-state outputs of open-loop reset systems into base-linear outputs and pulse-based nonlinear signals. Building on Theorem 1, Theorem 2 proposes an open-loop HOSIDF for the frequency response analysis of reset controllers.
2. Building upon the open-loop analysis in Theorem 2, Theorem 3 introduces a closed-loop analysis model for the Single-Sinusoid-Input Single-Output (SSISO) reset control system featuring two reset instants per steady-state period (referred to as a two-reset system). This model decomposes the closed-loop system's steady-state output into its base-linear and nonlinear components.
3. Based on Theorem 3, a closed-loop HOSIDF is developed for the frequency response analysis of reset control systems, as detailed in Theorem 4. This analysis connects the open-loop and closed-loop responses of reset control systems, enabling the application of loop-shaping techniques in nonlinear systems for the first time.

Section 5 assesses the accuracy and highlights limitations of the proposed methods on a reset control system within the PID framework, demonstrated through simulations and experiments. In Section 6, a two-reset control structure is proposed to address the limitations identified in Section 5. Simulated and experimental results on this new control system validate the effectiveness of the proposed analysis methods. Additionally, this section discusses the application of the proposed methods in reset control system design. Finally, the study concludes in Section 7.

2. Background and problem statement

This section begins by offering background information on reset control systems. It then discusses existing frequency response analysis methods for reset systems, highlighting their limitations. Finally, the research problems are introduced.

2.1. The definition of the reset control system

Fig. 1 shows the block diagram of the Single-Input Single-Output (SISO) reset control system. This system consists of a reset controller C, a Linear Time-Invariant (LTI) system C_α, a plant P, and a feedback loop. The blue lines depict the resetting mechanism activated by the reset trigger signal (which is $e(t)$ in this diagram). The signals $r(t)$, $e(t)$, $v(t)$, $u(t)$, and $y(t)$ correspond to the reference input signal, the error signal, the reset output signal, the control input signal, and the output signal, respectively. In the reset system under a sinusoidal input signal $r(t) = |R|\sin(\omega t)$ $(\omega \in \mathbb{R}^+)$, these signals are functions of both time t and input frequency ω. In the time domain, they are expressed as functions of t for a specific ω for simplicity. Under the condition of the existence of steady states, in the Fourier domain, $R(\omega)$, $E(\omega)$, $V(\omega)$, $U(\omega)$, and $Y(\omega)$ represent their respective Fourier transforms.

The state-space equations of the reset controller C in Fig. 1 are given by:

$$C = \begin{cases} \dot{x}_c(t) = A_R x_c(t) + B_R e(t), & t \notin J, \\ x_c(t^+) = A_\rho x_c(t), & t \in J, \\ v(t) = C_R x_c(t) + D_R e(t). \end{cases} \tag{1}$$

In (1), $x_c(t) \in \mathbb{R}^{n_c \times 1}$ represents the state of the reset controller C, where n_c denotes the number of states. The matrices $A_R \in \mathbb{R}^{n_c \times n_c}$, $B_R \in \mathbb{R}^{n_c \times 1}$, $C_R \in \mathbb{R}^{1 \times n_c}$, and $D_R \in \mathbb{R}^{1 \times 1}$ describe the continuous dynamics of the base-linear controller (BLC), denoted as $C_{bl}(\omega)$, given by

$$C_{bl}(\omega) = C_R(j\omega I - A_R)^{-1}B_R + D_R, \ (j = \sqrt{-1}). \tag{2}$$

The base-linear system (BLS) of the reset control system in Fig. 1 is the system characterized by substituting the reset controller C with its base-linear counterpart C_{bl}.

The reset controller employs the "zero-crossing law" as the reset mechanism, which enables the state $x_c(t)$ of C resets to a predetermined value whenever the reset-triggered signal crosses zero (Banos & Barreiro, 2012; Guo & Chen, 2019). In Fig. 1, the reset triggered signal is $e(t)$. The second equation in (1) describes the reset action, which is an instantaneous or impulsive change of the state $(x_c(t) \to x_c(t^+))$ applied whenever $e(t_i) = 0$ (Barreiro et al., 2014). The reset instant, denoted as t_i, is defined as the time at which the reset condition is satisfied, i.e., $e(t_i) = 0$. The set of reset instants for C is defined as $J := \{t_i | e(t_i) = 0, \ i \in \mathbb{Z}^+\}$. The symbol A_ρ represents the reset matrix, given by

$$A_\rho = \begin{bmatrix} \gamma & \\ & I_{n_l} \end{bmatrix} \in \mathbb{R}^{n_c \times n_c}, \tag{3}$$

where $\gamma = \text{diag}(\gamma_1, \gamma_2, \ldots, \gamma_o, \ldots, \gamma_{n_r})$, $o \in \mathbb{Z}^+$. $\gamma_o \in (-1, 1)$ denotes the ratio of the after-reset state value (at t_i^+) to the before-reset state value (at t_i). The subscripts n_r and n_l denote the numbers of reset states and non-reset (linear) states, respectively, where $n_c = n_r + n_l$. When $\gamma = I_{n_r}$, the reset controller C is referred to as its BLC C_{bl}. This study specifically focuses on the reset controller C that employs the "Zero-crossing Law" and involves a single reset state, where $n_r = 1$ in (3). The reset controllers with $n_r = 1$ encompass common elements such as the CI, the FORE, and the higher-order reset elements like the "Second-Order Single State Reset Element (SOSRE)" (Karbasizadeh et al., 2021).

In Fig. 1, the linear controller C_α combined with the plant $\mathcal{P}$ is defined as $\mathcal{P}_\alpha = C_\alpha \mathcal{P}$. The state-space representation of $\mathcal{P}_\alpha$ is defined as:

$$\mathcal{P}_\alpha = \begin{cases} \dot{x}_\alpha(t) = A_\alpha x_\alpha(t) + B_\alpha v(t), \\ y_\alpha(t) = C_\alpha x_\alpha(t), \end{cases} \tag{4}$$

where $A_\alpha \in \mathbb{R}^{n_\alpha \times n_\alpha}$, $B_\alpha \in \mathbb{R}^{n_\alpha \times 1}$, and $C_\alpha \in \mathbb{R}^{1 \times n_\alpha}$ are the state-space matrices for $\mathcal{P}_\alpha$. $x_\alpha \in \mathbb{R}^{n_\alpha \times 1}$ represents the state of $\mathcal{P}_\alpha$ and $n_\alpha \in \mathbb{N}$ is the number of the state.

Combining (1) and (4), the state-space representative of the reset control system without inputs is given by

$$\mathcal{H} = \begin{cases} \dot{x}(t) = A_{cl} x(t), & x \notin J_H, \\ x(t^+) = A_{\rho cl} x(t), & x \in J_H, \\ y(t) = C_{cl} x(t), \end{cases} \tag{5}$$

where $x^T = [x_c{}^T \; x_\alpha{}^T] \in \mathbb{R}^{n_s \times 1}$ is the state of the reset control system $\mathcal{H}$, with the number of $n_s = n_c + n_\alpha$. $J_H := \{x \in \mathbb{R}^{n_s \times 1} | C_{cl} x = 0\}$ is defined to be the set of reset instants satisfying $e(t) = 0$. The matrices in (5) are given by

$$\begin{aligned} A_{cl} &= \begin{bmatrix} A_R & -B_R C_\alpha \\ B_\alpha C_R & A_\alpha \end{bmatrix} \in \mathbb{R}^{n_s \times n_s}, \\ C_{cl} &= \begin{bmatrix} 0^{1 \times n_c} & C_\alpha \end{bmatrix} \in \mathbb{R}^{1 \times n_s}, \\ A_{\rho cl} &= \begin{bmatrix} A_\rho & 0 \\ 0 & I_{n_\alpha} \end{bmatrix} \in \mathbb{R}^{n_s \times n_s}. \end{aligned} \tag{6}$$

2.2. The stability and convergence conditions for reset systems

The stability and convergence of systems are crucial for achieving a steady-state solution and enabling frequency response to sinusoidal inputs (Pavlov et al., 2007, 2006). The reset system (1) with input signal of $e(t) = |E| \sin(\omega t + \angle E)$, $\omega > 0$ has a globally asymptotically stable $2\pi/\omega$-periodic solution if and only if (Guo et al., 2009)

$$|\lambda(D_R e^{A_R \delta})| < 1, \; \forall \delta \in \mathbb{R}^+, \tag{7}$$

where $\lambda(\cdot)$ represents the eigenvalues of the matrix. where $\lambda(\cdot)$ represents the eigenvalues of the matrix. Thus, to ensure the existence of steady-state solutions for the frequency response analysis of open-loop reset control system, the following assumption is made:

Assumption 1. The reset system (1) with input $e(t) = |E| \sin(\omega t + \angle E)$ meets the condition in (7). The LTI system C_α is Hurwitz.

The closed-loop reset control system (5) is quadratically stable if and only if it satisfies the well-known H_β condition (Beker et al., 2004; Carrasco et al., 2008), i.e., there exists a $\beta \in \mathbb{R}^{n_r \times 1}$ and a positive definite matrix $P_{n_r} \in \mathbb{R}^{n_r \times n_r}$ such that the transfer function

$$H_\beta(s) \overset{\Delta}{=} \begin{bmatrix} P_{n_r} & 0_{n_r \times n_l} & \beta C_\alpha \end{bmatrix} (sI - A_{cl})^{-1} \begin{bmatrix} I_{n_r} \\ 0_{n_l \times n_r} \\ 0_{n_\alpha \times n_r} \end{bmatrix} \tag{8}$$

is strictly positive real and additionally a non-zero reset matrix γ in (3) satisfies the condition

$$\gamma^T P_{n_r} \gamma - P_{n_r} \leqslant 0, \tag{9}$$

where I_{n_r} is an identity matrix of size $n_r \times n_r$.

Referring to the literature (Dastjerdi et al., 2022), the following assumption for the uniformly exponential convergence of closed-loop reset systems (5) is made:

Assumption 2. The closed-loop reset control system (5) is assumed to satisfy the following conditions: the initial condition of the reset controller C is zero, there are infinitely many reset instants t_i with $\lim_{t_i \to \infty} = \infty$, the input signal is a Bohl function (Barabanov & Konyukh, 2001), there is no Zeno behavior, and the H_β condition (in (8) and (9)) is satisfied.

The Assumption 2 can be met through appropriate design considerations, as detailed in Banos and Barreiro (2012), Saikumar et al. (2021), Samad et al. (2019).

The closed-loop reset control system (5) under a sinusoidal input signal $r(t) = |R| \sin(\omega t)$, satisfying Assumption 2, exhibits a periodic steady-state solution. This solution can be represented as $x(t) = S(\sin(\omega t), \cos(\omega t), \omega)$ for some function $S : \mathbb{R}^3 \to \mathbb{R}^{n_c + n_\alpha}$ (Dastjerdi et al., 2022).

Hybrid systems may encounter the Zeno phenomenon, where infinitely many actions occur within a finite time span (Wang et al., 2014). According to research (Barreiro et al., 2014), the outputs of a reset system are Zeno-free (non-Zeno) if the reset time interval $\sigma_i = t_{i+1} - t_i$, $i \in \mathbb{Z}^+$ between any two consecutive reset instants (t_i, t_{i+1}) is lower bounded:

$$\sigma_i > \sigma_{\min}, \; \sigma_{\min} \in \mathbb{R}^+, \tag{10}$$

at least in some working domain Ω (Barreiro et al., 2014).

2.3. Current frequency response analysis of the open-loop reset system

For an open-loop reset controller C (1), with the input signal and the reset triggered signal of $e(t) = |E| \sin(\omega t)$ and satisfying Assumption 1, there exist $n \in \mathbb{N}$ harmonics in the reset output signal $v(t)$. Utilizing the "Virtual Harmonic Generator" (Heinen, 2018), the input signal $e(t)$ generates n harmonics $e_{1n}(t) = |E| \sin(n\omega t)$. The function $H_n(\omega)$, where n denotes the number of harmonics involved, is defined to represent the transfer function from $e_{1n}(t)$ to the nth harmonic in $v(t)$ at steady states. The expression for $H_n(\omega)$ is provided by Heinen (2018), Saikumar et al. (2021):

$$H_n(\omega) = \begin{cases} C_R(j\omega I - A_R)^{-1}(I + j\Theta_D(\omega))B_R + D_R, & \text{for } n = 1, \\ C_R(jn\omega I - A_R)^{-1} j\Theta_D(\omega) B_R, & \text{for odd } n > 1, \\ 0, & \text{for even } n \geqslant 2, \end{cases} \tag{11}$$

with

$$\begin{aligned} \Lambda(\omega) &= \omega^2 I + A_R{}^2, \\ \Delta(\omega) &= I + e^{(\frac{\pi}{\omega} A_R)}, \\ \Delta_r(\omega) &= I + A_\rho e^{(\frac{\pi}{\omega} A_R)}, \\ \Gamma_r(\omega) &= \Delta_r^{-1}(\omega) A_\rho \Delta(\omega) \Lambda^{-1}(\omega), \\ \Theta_D(\omega) &= \frac{-2\omega^2}{\pi} \Delta(\omega)[\Gamma_r(\omega) - \Lambda^{-1}(\omega)]. \end{aligned} \tag{12}$$

The expression for the first-order harmonic $H_1(\omega)$ aligns with the classical DF representation for the reset controller in Guo et al. (2009).

2.4. Problem statement

Under Assumption 2, in a SISO closed-loop reset control system with a sinusoidal reference input signal $r(t) = |R| \sin(\omega t)$ (in Fig. 1), the steady-state signals $e(t)$, $v(t)$, $u(t)$, and $y(t)$ are periodic and nonlinear. The Fourier transformations of these signals are define as $E(\omega)$, $V(\omega)$, $U(\omega)$, and $Y(\omega)$, respectively. These signals encompass infinite harmonics and share the fundamental frequency of $r(t)$ (Pavlov et al., 2006).

They can be expressed as follows:

$$\begin{aligned} e(t) &= \sum_{n=1}^{\infty} e_n(t) = \sum_{n=1}^{\infty} |E_n| \sin(n\omega t + \angle E_n), \\ v(t) &= \sum_{n=1}^{\infty} v_n(t) = \sum_{n=1}^{\infty} |V_n| \sin(n\omega t + \angle V_n), \\ u(t) &= \sum_{n=1}^{\infty} u_n(t) = \sum_{n=1}^{\infty} |U_n| \sin(n\omega t + \angle U_n), \\ y(t) &= \sum_{n=1}^{\infty} y_n(t) = \sum_{n=1}^{\infty} |Y_n| \sin(n\omega t + \angle Y_n), \end{aligned} \tag{13}$$

where $\angle E_n$, $\angle V_n$, $\angle U_n$, $\angle Y_n \in (-\pi, \pi]$. The signals $e_n(t)$, $v_n(t)$, $u_n(t)$ and $y_n(t)$ are the nth harmonics of $e(t)$, $v(t)$, $u(t)$ and $y(t)$, respectively. The Fourier transformations of these signals are define as $E_n(\omega)$, $V_n(\omega)$, $U_n(\omega)$, and $Y_n(\omega)$, respectively. Conducting a frequency response analysis is an effective method for understanding the frequency-domain dynamics of closed-loop reset control systems (Saikumar et al., 2021). For instance, the low-frequency sensitivity function of the system serves as a crucial metric for assessing the tracking precision of the system. Currently, two frequency response analysis methods for closed-loop reset control systems are available, denoted as Method A and Method B.

Method A (Guo et al., 2009): For a SISO reset system with a reference input signal $r(t) = |R| \sin(\omega t)$ under Assumption 2, as shown in Fig. 1, the sensitivity function $S_{DF}(\omega)$, complementary sensitivity function $\mathcal{T}_{DF}(\omega)$, and control sensitivity function $CS_{DF}(\omega)$ based on the steady-state DF analysis are defined as

$$\begin{aligned} S_{DF}(\omega) &= \frac{E(\omega)}{R(\omega)} = \frac{1}{1 + H_1(\omega)C_\alpha(\omega)\mathcal{P}(\omega)}, \\ \mathcal{T}_{DF}(\omega) &= \frac{Y(\omega)}{R(\omega)} = \frac{H_1(\omega)\mathcal{P}(\omega)}{1 + H_1(\omega)C_\alpha(\omega)\mathcal{P}(\omega)}, \\ CS_{DF}(\omega) &= \frac{U(\omega)}{R(\omega)} = \frac{H_1(\omega)C_\alpha(\omega)}{1 + H_1(\omega)C_\alpha(\omega)\mathcal{P}(\omega)}, \end{aligned} \tag{14}$$

where $H_1(\omega)$ represents the first-order harmonic transfer function of C, as defined in (11). However, Method A is inaccurate for predicting the performance of closed-loop reset control systems since it only considers the first-order harmonic of the reset control system, thus being valid only when $e_n(t) = 0$ for $n > 1$ in (13). In contrast, the following Method B incorporates the higher-order harmonics, which is more accurate.

Method B (Saikumar et al., 2021): For a SISO reset control system in Fig. 1 with a reference input signal $r(t) = |R| \sin(\omega t)$, under three assumptions: (1) Assumption 2, (2) the reset triggered signal is $e_1(t)$ which results in two reset instants occurring π/ω apart per cycle, and (3) the error $e_n(t)$ for $n > 1$ does not undergo reset actions, the n^{th} ($n \in \mathbb{N}$) steady-state sensitivity function, complementary sensitivity function, and control sensitivity function denoted as $S_n(\omega)$, $\mathcal{T}_n(\omega)$, and $CS_n(\omega)$ are given by

$$\begin{aligned} S_n(\omega) &= \frac{E_n(n\omega)}{R_n(\omega)} = \begin{cases} S_{l1}(\omega), & \text{for } n = 1, \\ -\mathcal{L}_n(\omega)S_{bl}(n\omega)(\left|S_{l1}(\omega)\right| \angle(n\angle S_{l1}(\omega))), & \text{for odd } n > 2, \\ 0, & \text{for even } n \geqslant 2, \end{cases} \\ \mathcal{T}_n(\omega) &= \frac{Y_n(n\omega)}{R_n(\omega)} = \begin{cases} 1 - S_{l1}(\omega), & \text{for } n = 1, \\ \mathcal{L}_n(\omega)S_{bl}(n\omega)(\left|S_{l1}(\omega)\right| \angle(n\angle S_{l1}(\omega))), & \text{for odd } n > 2, \\ 0, & \text{for even } n \geqslant 2, \end{cases} \\ CS_n(\omega) &= \frac{U_n(n\omega)}{R_n(\omega)} = \mathcal{T}_n(\omega)/\mathcal{P}(n\omega), \end{aligned} \tag{15}$$

where

$$\begin{aligned} S_{ln}(\omega) &= 1/(1 + \mathcal{L}_n(\omega)), \\ R_n(\omega) &= |R|\mathcal{F}[\sin(n\omega t)], \\ S_{bl}(n\omega) &= 1/(1 + \mathcal{L}_{bl}(n\omega)), \\ \mathcal{L}_n(\omega) &= H_n(\omega)C_\alpha(n\omega)\mathcal{P}(n\omega), \\ \mathcal{L}_{bl}(n\omega) &= C_{bl}(n\omega)C_\alpha(n\omega)\mathcal{P}(n\omega). \end{aligned} \tag{16}$$

The first-order harmonic in Method B is identical to Method A. Although Method B takes the higher-order harmonics (for $n > 1$) into consideration, Assumption 3 overlooks the higher-order harmonics generated by $e_n(t)(n > 1)$ in (13). This oversight will result in analysis inaccuracies in $S_n(\omega)$, $\mathcal{T}_n(\omega)$, and $CS_n(\omega)$ in (15), motivating the contributions made in this paper. The main idea of this paper is to introduce new methods for analyzing the open-loop and closed-loop frequency responses of SISO reset control systems depicted in Fig. 1. The study begins with the open-loop analysis of the reset controller by presenting a novel analytical method to decompose the steady-state outputs $v(t)$ of the reset controller C in Fig. 1 under sinusoidal inputs into its base-linear component $v_{bl}(t)$ and pulse-based nonlinear components $v_{nl}(t)$, given by:

$$v(t) = v_{bl}(t) + v_{nl}(t).$$

The detailed expressions for $v_{bl}(t)$ and $v_{nl}(t)$ will be provided in Section 3. This decomposition approach facilitates the development of new open-loop frequency response analysis for the reset controller C, decomposed into its base-linear controller C_{bl} and nonlinear elements in the frequency domain.

The proposed open-loop analysis enables the development of a closed-loop frequency response analysis method, which will be provided in Section 4. This closed-loop analysis addresses inaccuracies in previous methods, particularly correcting the assumptions (Assumption 3) in Method B (Saikumar et al., 2021), by introducing new sensitivity functions $S_n(\omega)$, $\mathcal{T}_n(\omega)$, and $CS_n(\omega)$ for reset control systems. These functions describe the sensitivity of the closed-loop reset systems to input variations in the frequency domain, including higher-order harmonics. Furthermore, the sensitivity functions effectively connect the frequency-domain open-loop analysis and closed-loop analysis. Finally, simulations and experiments on a precision motion stage validate the effectiveness of these analysis methods.

3. The frequency response analysis for the open-loop reset system

This section introduces a pulse-based analysis model for the open-loop reset controller at steady states. The model separates the output of a SSISO reset controller into its base-linear sinusoidal output and a filtered pulse signal. The term "filtered pulse signal" refers to a signal obtained by filtering a normalized pulse signal through a finite-dimensional LTI transfer function.

The reset controller C (1) is based on the classical Clegg integrator (CI) (Banos & Barreiro, 2012). To develop the analysis model for a generalized reset controller, the study first focuses on analyzing the CI. The Generalized CI (GCI) is defined as the reset controller C (1) with $A_R = 0$, $B_R = 1$, $C_R = 1$, $D_R = 0$, and $A_\rho = \gamma \in (-1, 1)$, under Assumption 1 and the Zeno-free condition in (10). Lemma 1 illustrates that the output of the GCI under a sinusoidal input is the sum of its base-linear output and a square wave component.

Lemma 1 (*The Pulse-Based Model for the Open-Loop GCI*). *For a GCI subjected to a sinusoidal input signal $e(t) = |E_1| \sin(\omega t)$, its steady-state output signal denoted by $u_{ci}(t)$ consists of two components: one is its base-linear output $u_i(t)$ and another is a square wave represented as $q_i(t)$, expressed by:*

$$u_{ci}(t) = u_i(t) + q_i(t), \tag{17}$$

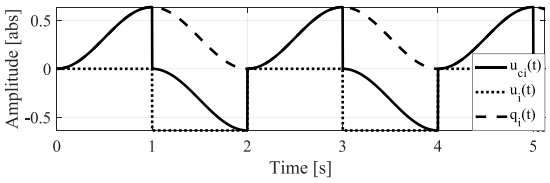

Fig. 2. $u_{ci}(t)$ (solid line), $u_i(t)$ (dotted line), and $q_i(t)$ (dashed line) of open-loop CI.

where $u_i(t) = -|E_1|[\cos(\omega t) - 1]/\omega$, *and* $q_i(t)$ *is a* $2\pi/\omega$*-periodical square wave given by*

$$q_i(t) = \begin{cases} -2|E_1|\gamma(\gamma+1)^{-1}/\omega, & \text{for } t \in [2k, 2k+1)\cdot\pi/\omega, \\ -2|E_1|(\gamma+1)^{-1}/\omega, & \text{for } t \in [2k+1, 2k+2)\cdot\pi/\omega, \end{cases} \tag{18}$$

where $k \in \mathbb{N}$.

Proof. The proof can be found in Appendix A. □

Fig. 2 displays the simulation results of an open-loop CI with the input signal $e(t) = \sin(\omega t)$ ($\omega = \pi$ rad/s and $\gamma = 0$). In this case, $q_i(t)$ is a square wave with a period of 2 s and amplitudes of 0 and 0.64, as calculated by (18).

Theorem 1 extends the pulse-based analysis model from the GCI to an open-loop reset controller C (1), where the input and reset-triggered signals are different .

Theorem 1 (*The Pulse-Based Analysis Model for the Open-Loop Reset Controller*)**.** *Consider a reset controller* C *described by* (1)*, where* $n_r = 1$*, subject to a sinusoidal input signal* $e(t) = |E_n|\sin(n\omega t + \angle E_n)$ *with* $\angle E_n \in (-\pi, \pi]$ *and* $n = 2k+1$ *for* $k \in \mathbb{N}$*, along with a* $2\pi/\omega$*-periodic reset triggered signal denoted by* $e_s(t) = |E_s|\sin(\omega t + \angle E_s)$*, where* $\angle E_s \in (-\pi, \pi]$*, meeting the condition in* (7) *and adhere to the Zeno-free condition outlined in* (10)*. The input signal* $e(t) = |E_n|\sin(n\omega t + \angle E_n)$ *varies as a function of time* t*, while the parameters* ω *and* n *remain constant. The steady-state reset output* $v(t)$ *is expressed as:*

$$v(t) = v_{bl}(t) + v_{nl}(t), \tag{19}$$

where $v_{bl}(t)$ *is the steady-state base-linear output given by*

$$v_{bl}(t) = |E_n C_{bl}(n\omega)|\sin(n\omega t + \angle E_n + \angle C_{bl}(n\omega)). \tag{20}$$

The nonlinear signal $v_{nl}(t)$ *shares the same phase and period as the reset-triggered signal* $e_s(t)$*, as obtained by*

$$v_{nl}(t) = \sum_{\mu=1}^{\infty} \mathscr{F}^{-1}[\Delta_x(\mu\omega)Q^{\mu}(\omega)],\ \mu = 2k+1,\ k \in \mathbb{N}, \tag{21}$$

where

$$\begin{aligned} \Delta_l(n\omega) &= (jn\omega I - A_R)^{-1}B_R, \\ \Delta_x(\mu\omega) &= C_R(j\mu\omega I - A_R)^{-1}j\mu\omega I, \\ \Delta_c^n(\omega) &= |\Delta_l(n\omega)|\sin(\angle\Delta_l(n\omega) + \angle E_n - n\angle E_s), \\ Q^{\mu}(\omega) &= 2|E_n|\Delta_q^n(\omega)\mathscr{F}[\sin(\mu\omega t + \mu\angle E_s)]/(\mu\pi), \\ \Delta_q^n(\omega) &= (I + e^{A_R\pi/\omega})(A_\rho e^{A_R\pi/\omega} - I)^{-1}(I - A_\rho)\Delta_c^n(\omega). \end{aligned} \tag{22}$$

Proof. The proof is provided in Appendix B. □

The reset controller C in Fig. 1 with the same input signal and reset-triggered signal $e(t) = |E_1|\sin(\omega t + \angle E_1)$, corresponds to the reset controller discussed in Theorem 1 when $e_s(t) = e(t)$. Based on Theorem 1, Theorem 2 presents the Higher-order Sinusoidal Input Describing Function (HOSIDF) for the open-loop reset controller C in Fig. 1. The corresponding HOSIDF block diagram for C is depicted in Fig. 3.

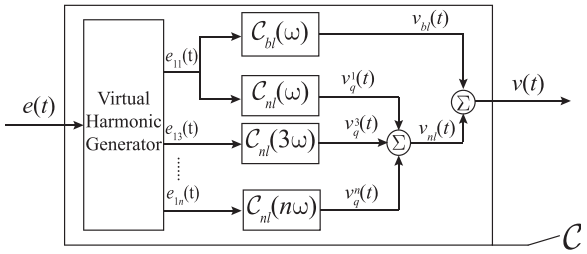

Fig. 3. The HOSIDF block diagram of an open-loop reset controller C.

Theorem 2 (*The HOSIDF for the Open-Loop Reset Controller*)**.** *Consider a reset controller* C (1) *with one reset state where* $n_r = 1$ *in response to the input signal and reset-triggered signal* $e(t) = |E_1|\sin(\omega t + \angle E_1)$*,* $(\angle E_1 \in (-\pi, \pi])$*, meeting the condition in* (7) *and satisfying the Zeno-free condition in* (10)*. The steady-state output signal* $v(t)$ *comprises* $n \in \mathbb{N}$ *harmonics, expressed as* $v(t) = \sum_{n=1}^{\infty} v_n(t)$*, with the Fourier transform defined as* $V(\omega) = \sum_{n=1}^{\infty} V_n(\omega)$*. In Fig. 3, the application of the "Virtual Harmonic Generator" (Nuij et al., 2006; Saikumar et al., 2021) introduces* $e_{1n}(t) = |E_1|\sin(n\omega t + n\angle E_1)$*, with Fourier transform denoted as* $E_{1n}(\omega)$*. The* n*th steady-state transfer function of* C*, denoted as* $C_n(\omega)$*, represents the ratio of* $V_n(\omega)$ *to* $E_{1n}(\omega)$ *and is given by:*

$$C_n(\omega) = \frac{V_n(\omega)}{E_{1n}(\omega)} = \begin{cases} C_{bl}(\omega) + C_{nl}(\omega), & \text{for } n = 1, \\ C_{nl}(n\omega), & \text{for odd } n > 1, \\ 0, & \text{for even } n \geq 2, \end{cases} \tag{23}$$

where $C_{bl}(\omega)$ *is the base-linear transfer function given in* (2) *and* $C_{nl}(n\omega)$ *is derived by*

$$\begin{aligned} \Delta_l(\omega) &= (j\omega I - A_R)^{-1}B_R, \\ \Delta_q(\omega) &= (I + e^{A_R\pi/\omega})\Delta_v(\omega), \\ \Delta_c(\omega) &= |\Delta_l(\omega)|\sin(\angle\Delta_l(\omega)), \\ C_{nl}(n\omega) &= 2\Delta_x(n\omega)\Delta_q(\omega)/(n\pi), \\ \Delta_x(n\omega) &= C_R(jn\omega I - A_R)^{-1}jn\omega I, \\ \Delta_v(\omega) &= (A_\rho e^{A_R\pi/\omega} - I)^{-1}(I - A_\rho)\Delta_c(\omega). \end{aligned} \tag{24}$$

Proof. The proof can be found in Appendix C. □

Corollary 1. *Consider a reset controller* C (1) *with one reset state where* $n_r = 1$ *in response to the input signal and reset-triggered signal* $e(t) = |E_1|\sin(\omega t + \angle E_1)$*,* $(\angle E_1 \in (-\pi, \pi])$*. The reset controller* C (1) *operates under the condition in* (7) *and satisfies the Zeno-free condition in* (10)*. The steady-state reset output signal* $v(t)$ *is expressed as:*

$$v(t) = v_{bl}(t) + v_{nl}(t), \tag{25}$$

where $v_{bl}(t)$ *is the steady-state base-linear output given by*

$$v_{bl}(t) = |E_1 C_{bl}(\omega)|\sin(\omega t + \angle C_{bl}(\omega)). \tag{26}$$

The nonlinear signal $v_{nl}(t)$ *is given by*

$$v_{nl}(t) = \sum_{n=1}^{\infty} \mathscr{F}^{-1}[E_{1n}(\omega)C_{nl}(n\omega)]. \tag{27}$$

Proof. The proof is provided in Appendix D. □

Note that the prior work (Kaczmarek et al., 2022) introduced the pulse-based model for the open-loop reset controller but did not extend this model to include a frequency-domain analysis for the controller. Theorem 2 completes this research and presents a new HOSIDF for analyzing the open-loop reset controller.

Applying Theorem 2, Remark 1 provides the analysis for the open-loop reset control system in Fig. 1.

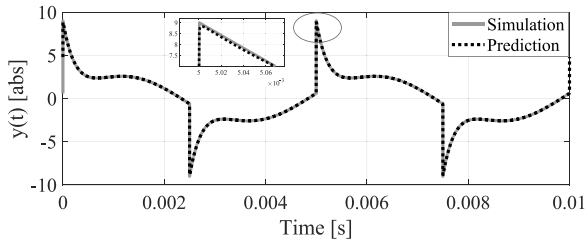

Fig. 4. The comparison between the simulated and Theorem 2-predicted output signals in a reset control system.

Remark 1. For an open-loop reset control system in Fig. 1 with the sinusoidal input signal $e(t) = |E_1|\sin(\omega t + \angle E_1)$ and under Assumption 1, the transfer function $\mathcal{L}_n(\omega)$, $n \in \mathbb{N}$ from the input $e(t)$ to the steady-state output $y(t)$ is composed of a linear transfer function $\mathcal{L}_{bl}(\omega)$ and nonlinear transfer functions $\mathcal{L}_{nl}(n\omega)$, given by

$$\mathcal{L}_n(\omega) = \begin{cases} \mathcal{L}_{bl}(\omega) + \mathcal{L}_{nl}(\omega), & \text{for } n = 1, \\ \mathcal{L}_{nl}(n\omega), & \text{for odd } n > 1, \\ 0, & \text{for even } n \geqslant 2, \end{cases} \tag{28}$$

with

$$\begin{aligned} \mathcal{L}_{bl}(n\omega) &= C_{bl}(n\omega)C_\alpha(n\omega)\mathcal{P}(n\omega), \\ \mathcal{L}_{nl}(n\omega) &= C_{nl}(n\omega)C_\alpha(n\omega)\mathcal{P}(n\omega), \end{aligned} \tag{29}$$

where $C_{bl}(n\omega)$ and $C_{nl}(n\omega)$ are given in (2) and (24), respectively.

From Eq. (28), the steady-state output signal $y(t)$ of the open-loop reset system is given by

$$\begin{aligned} y(t) &= \mathscr{F}^{-1}[E_{1n}(\omega)\mathcal{L}_n(\omega)], \\ E_{1n}(\omega) &= |E_1|\sin(n\omega t + n\angle E_1). \end{aligned} \tag{30}$$

To validate the accuracy of Theorem 2 and Remark 1, Fig. 4 compares the simulated and Eq. (30)-predicted output signals $y(t)$ in an reset control system with input signal of $e(t) = \sin(400\pi t)$. The parameters of the system are designed as: the reset controller has a base-linear transfer function $C_{bl}(s) = 1/(s/(300\pi) + 1)$ with $\gamma = 0$, $C_\alpha(s) = (s/(75\pi) + 1)/(s/(1200\pi) + 1)$, and $\mathcal{P}(s) = 1$.

The results demonstrate the accuracy of Theorem 2 and Remark 1. Note that that in the zoom-in plot, the slight discrepancy at the signal edges between the two plots arises from the consideration of 5000 harmonics during the calculation process, whereas the actual output comprises an infinite number of harmonics. The choice of the number of harmonics considered in the calculation allows readers to balance computation time and prediction precision.

The newly introduced HOSIDF $C_n(\omega)$ (23) is mathematically equivalent to the function $H_n(\omega)$ (11) when the input signal and reset-triggered signal for the reset controller are the same, denoted as $e(t) = |E_1|\sin(\omega t + \angle E_1)$. However, the new HOSIDF offers several new insights: (1) It facilitates the separation of the output $v(t)$ of the reset controller into linear $v_{bl}(t)$ (26) and nonlinear $v_{nl}(t)$ (27) components. Specifically, $v_{bl}(t)$ is derived from the base-linear transfer function $C_{bl}(\omega)$ (2), while $v_{nl}(t)$ is obtained from $C_{nl}(n\omega)$ (24). (2) The nonlinear signal $v_{nl}(t)$ is a filtered pulse signal that shares the same phase and period as the reset-triggered signal $e_s(t)$. (3) The magnitude of the signal $v_{nl}(t)$ is determined by $C_{nl}(n\omega)$. These insights enable the connection between open-loop analysis and closed-loop frequency analysis, as discussed in Section 4.

4. The frequency response analysis for the closed-loop reset system

Based on the open-loop analysis in Theorem 2, this section develops the closed-loop frequency response analysis for the reset control system depicted in Fig. 1.

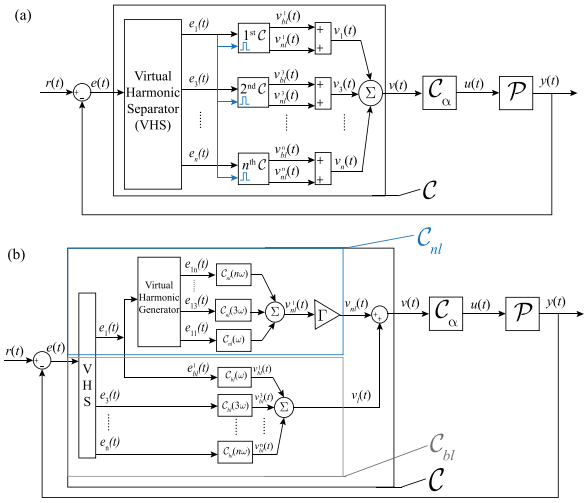

Fig. 5. Block diagrams for the closed-loop RCS, wherein (a) the resetting actions are indicated by the blue lines. In (b), the reset controller is decomposed into two components: the linear part C_{bl} within the gray box and the nonlinear part C_{nl} contained within the blue box. (For interpretation of the references to color in this figure legend, the reader is referred to the web version of this article.)

In a closed-loop reset control system under a sinusoidal input signal $r(t) = |R|\sin(\omega t)$ at steady states, a "two-reset system" is defined as a reset system having two reset instants per steady-state cycle, while a "multiple-reset system" involves more than two reset instants per steady-state cycle. In the two-reset system, the dominated component of the error signal $e(t)$ is the first-order harmonic $e_1(t)$ in (13). Multiple-reset actions, such as those implemented in the PI+CI control system, introduce excessive higher-order harmonics compared to two-reset actions (Baños & Vidal, 2007). This issue can be mitigated through careful design considerations (Karbasizadeh et al., 2022; Saikumar et al., 2019). Conditions for achieving periodic output in a multiple-reset system, where the interval between successive resets is not constant, are discussed in Beker (2001). Classical DF also assumes the $e_1(t)$ results in reset actions. Moreover, based on the authors' best knowledge, most practical reset control systems in the literature are designed to take advantage of two-reset systems (Banos & Barreiro, 2012). Given these insights, it is essential to explore frequency-domain analysis methods tailored to two-reset systems. Hence, the following assumption is introduced:

Assumption 3. There are two reset instants in a SISO closed-loop reset control system with a sinusoidal reference input signal $r(t) = |R|\sin(\omega t)$ at steady states, where the reset-triggered signal is $e_1(t)$.

Note that achieving Assumption 3 is feasible through practical reset control design. For instance, the CgLp reset element introduced in Saikumar et al. (2019) enables the realization of wide-band two-reset systems.

Under Assumptions 2 and 3, the reset actions in the closed-loop SISO reset control system occur when $e_1(t) = |E_1|\sin(\omega t + \angle E_1) = 0$, where $\angle E_1 \in (-\pi, \pi]$. The set of reset instants for this closed-loop reset system is denoted as $J_m := \{t_m = (m\pi - \angle E_1)/\omega | m \in \mathbb{Z}^+\}$. Since the reset interval $\sigma_m = t_{m+1} - t_m = \pi/\omega > \delta_{\min}$ (Barreiro et al., 2014), the trajectories for the reset system are Zeno-free.

Fig. 5(a) constructs the first block diagram for the closed-loop reset control system under Assumptions 2 and 3. In this block diagram, first, utilizing the "Virtual Harmonic Separator" (Nuij et al., 2006), the error signal $e(t)$ is decomposed into its harmonics, $e_n(t)$, as defined in (13). Next, each $e_n(t)$ is filtered by the reset controller C, resulting in a response denoted as $v_n(t)$. By summing up $v_n(t)$, the reset output signal $v(t)$ is obtained. In this context, C with the input signal $e_n(t)$ is referred

to as the nth reset controller. Theorem 1 illustrates that the steady-state output of a reset controller C under a sinusoidal input signal is composed of base-linear $v_{bl}(t)$ and nonlinear $v_{nl}(t)$ components.

Let $v_{bl}^n(t)$ and $v_{nl}^n(t)$ represent the steady-state base-linear and nonlinear output signals for the nth C. Then, the steady-state reset output signal $v(t)$ in the closed-loop reset system is given by:

$$\begin{aligned} v(t) &= \sum_{n=1}^{\infty} v_n(t), \\ v_n(t) &= v_{bl}^n(t) + v_{nl}^n(t). \end{aligned} \tag{31}$$

From (31), by defining

$$\begin{aligned} v_l(t) &= \sum_{n=1}^{\infty} v_{bl}^n(t), \\ v_{nl}(t) &= \sum_{n=1}^{\infty} v_{nl}^n(t), \end{aligned} \tag{32}$$

$v(t)$ can be written as

$$v(t) = v_l(t) + v_{nl}(t). \tag{33}$$

In the Fourier domain, Eq. (31) is expressed as

$$\begin{aligned} V(\omega) &= \sum_{n=1}^{\infty} V_n(\omega), \\ V_n(\omega) &= V_{bl}^n(\omega) + V_{nl}^n(\omega). \end{aligned} \tag{34}$$

Derived from (20), $V_{bl}^n(\omega)$ is given by

$$V_{bl}^n(\omega) = E_n(\omega) C_{bl}(n\omega). \tag{35}$$

Based on the block diagram for the closed-loop reset system shown in Fig. 5(a), Theorem 3 concludes the development of the pulse-based model for the closed-loop reset control system, visually represented in Fig. 5(b).

Theorem 3 (*The Pulse-Based Analysis Model for the Closed-Loop Reset System*). *In a closed-loop reset control system (with reset controller C (1) where $n_r = 1$), as depicted in Fig. 1 with a sinusoidal reference input signal $r(t) = |R|\sin(\omega t)$ and under Assumptions 2 and 3, the steady-state reset output signal $v(t)$ is expressed as:*

$$\begin{aligned} v(t) &= v_l(t) + v_{nl}(t), \\ v_l(t) &= \sum_{n=1}^{\infty} v_{bl}^n(t), \\ v_{nl}(t) &= \Gamma(\omega) \sum_{n=1}^{\infty} v_{nl}^1(t), \\ v_{bl}^n(t) &= \mathcal{F}^{-1}[E_n(\omega) C_{bl}(n\omega)], \\ v_{nl}^1(t) &= \sum_{n=1}^{\infty} \mathcal{F}^{-1}[E_{1n}(\omega) C_{nl}(n\omega)], \end{aligned} \tag{36}$$

where

$$\begin{aligned} \Delta_c^1(\omega) &= |\Delta_l(\omega)| \sin(\angle \Delta_l(\omega)), \\ E_{1n}(\omega) &= |E_1| \mathcal{F}^{-1}[\sin(n\omega t + n\angle E_1)], \\ \Gamma(\omega) &= 1/(1 - \sum_{n=3}^{\infty} \Psi_n(\omega) \Delta_c^n(\omega)/\Delta_c^1(\omega)), \\ \Psi_n(\omega) &= |\mathcal{L}_{nl}(n\omega)|/|1 + \mathcal{L}_{bl}(n\omega)|, \ n = 2k+1, \ k \in \mathbb{N}, \\ \Delta_c^n(\omega) &= -|\Delta_l(n\omega)| \sin(\angle \mathcal{L}_{nl}(n\omega) - \angle(1 + \mathcal{L}_{bl}(n\omega)) + \angle \Delta_l(n\omega)), \ \text{for } n > 1. \end{aligned} \tag{37}$$

Functions $C_{bl}(\omega)$, $C_{nl}(\omega)$, $\Delta_l(n\omega)$, $\mathcal{L}_{bl}(n\omega)$ and $\mathcal{L}_{nl}(n\omega)$ can be found in (2), (24), (22) and (29), respectively.

Proof. The proof is provided in Appendix E. □

Remark 2. From (32) and (36), $\Gamma(\omega)$ in (37) represents the ratio of $v_{nl}(t) = 1 + \sum_{n=3}^{\infty} v_{nl}^n(t)$ to $v_{nl}^1(t)$ at the input frequency ω. It serves as an indicator of the relative magnitude of higher-order harmonics $\sum_{n=3}^{\infty} v_{nl}^n(t)$ compared to the first-order harmonic $v_{nl}^1(t)$. A larger value of $\Gamma(\omega)$ indicates a relatively larger magnitude of higher-order harmonics in closed-loop reset systems.

Building upon the analytical model introduced in Theorem 3, a new Higher-Order Sinusoidal Input Describing Function (HOSIDF) for the frequency response analysis of closed-loop reset control systems is proposed. The detailed formulation is presented in Theorem 4.

Theorem 4 (*The Closed-Loop HOSIDF for SISO Reset Control Systems*). *Consider a closed-loop SISO reset control system in Fig. 1 with a reset controller C (1) (where $n_r = 1$) and to a sinusoidal reference input signal $r(t) = |R|\sin(\omega t)$. This system complies with Assumptions 2 and 3. By employing the "Virtual Harmonics Generator" to the input signal $r(t)$, the signal $r_n(t) = |R|\sin(n\omega t)$, $n \in \mathbb{N}$ is introduced, along with its Fourier transform $R_n(\omega)$. The transfer functions $\mathcal{S}_n(\omega)$, $\mathcal{T}_n(\omega)$, and $C\mathcal{S}_n(\omega)$ of the closed-loop reset system at steady states are defined as follows:*

$$\mathcal{S}_n(\omega) = \frac{E_n(\omega)}{R_n(\omega)} = \begin{cases} \frac{1}{1+\mathcal{L}_o(\omega)}, & \text{for } n = 1, \\ -\frac{\Gamma(\omega)\mathcal{L}_{nl}(n\omega)|S_1(\omega)|e^{jn\angle S_1(\omega)}}{1+\mathcal{L}_{bl}(n\omega)}, & \text{for odd } n > 1, \\ 0, & \text{for even } n \geqslant 2, \end{cases} \tag{38}$$

$$\mathcal{T}_n(\omega) = \frac{Y_n(\omega)}{R_n(\omega)} = \begin{cases} \frac{\mathcal{L}_o(\omega)}{1+\mathcal{L}_o(\omega)}, & \text{for } n = 1, \\ \frac{\Gamma(\omega)\mathcal{L}_{nl}(n\omega)|S_1(\omega)|e^{jn\angle S_1(\omega)}}{1+\mathcal{L}_{bl}(n\omega)}, & \text{for odd } n > 1, \\ 0, & \text{for even } n \geqslant 2, \end{cases} \tag{39}$$

$$C\mathcal{S}_n(\omega) = \frac{U_n(\omega)}{R_n(\omega)} = \frac{\mathcal{T}_n(\omega)}{\mathcal{P}(n\omega)}, \tag{40}$$

where

$$\begin{aligned} R_n(\omega) &= |R| \mathcal{F}[\sin(n\omega t)], \\ \mathcal{L}_o(n\omega) &= \mathcal{L}_{bl}(n\omega) + \Gamma(\omega)\mathcal{L}_{nl}(n\omega). \end{aligned} \tag{41}$$

Functions $\mathcal{L}_{bl}(n\omega)$, $\mathcal{L}_{nl}(n\omega)$, and $\Gamma(\omega)$ are given in (29) and (37).

Proof. The proof is provided in Appendix F. □

Remark 3. Consider a SISO reset control system under Assumption 2 and with a sinusoidal reference signal $r(t) = |R|\sin(\omega t)$, as depicted in Fig. 1. By utilizing the "Virtual Harmonic Generator", the input signal $r(t)$ generates $n = 2k+1 (k \in \mathbb{N})$ harmonics $r_n(t) = |R|\sin(n\omega t)$. The Fourier transform for $r_n(t)$ is denoted as $R_n(\omega)$. The steady-state error signal $e(t)$, output signal $y(t)$, and control input signal $u(t)$ are expressed as follows:

$$\begin{aligned} e(t) &= \sum_{n=1}^{\infty} e_n(t) = \sum_{n=1}^{\infty} \mathcal{F}^{-1}\left[\mathcal{S}_n(\omega) R_n(\omega)\right], \\ y(t) &= \sum_{n=1}^{\infty} y_n(t) = \sum_{n=1}^{\infty} \mathcal{F}^{-1}\left[\mathcal{T}_n(\omega) R_n(\omega)\right], \\ u(t) &= \sum_{n=1}^{\infty} u_n(t) = \sum_{n=1}^{\infty} \mathcal{F}^{-1}\left[C\mathcal{S}_n(\omega) R_n(\omega)\right]. \end{aligned} \tag{42}$$

Remark 4. The function $\Gamma(\omega)$ in (37), represents the ratio of the nonlinear outputs $v_{nl}(t)$ to $v_{nl}^1(t)$ in (36) at input frequency ω. Previous frequency response analysis methods, Method A and Method B, introduced in Section 2.4, assume that the higher-order harmonics $v_{nl}^n(t)$ (for $n > 1$) generated by $e_n(t)$ are zero, thereby implying $\Gamma(\omega) = 1$. However, this assumption does not hold across the entire frequency spectrum of the reset control system, leading to inaccuracies in the analysis. Theorem 4 addresses these inaccuracies analytically by introducing $\Gamma(\omega)$ in (37). While Theorem 4 exhibits comparable accuracy to Method

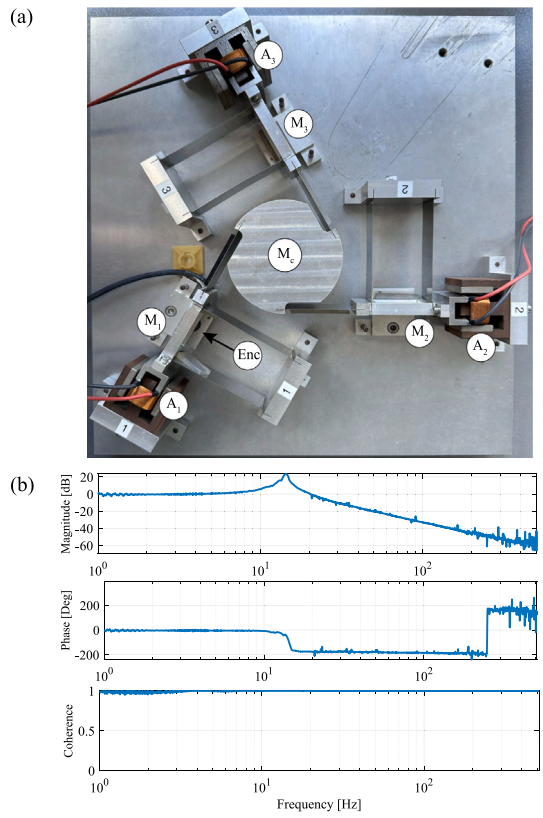

Fig. 6. (a) The planar precision positioning system. (b) The FRF data from actuator A_1 to attached mass M_1.

B within the frequency range where $\Gamma(\omega) = 1$, it has superior accuracy compared to Method B when $\Gamma(\omega) \neq 1$, particularly in scenarios where the magnitudes of higher-order harmonics $v_{nl}^{n}(t)$ (for $n > 1$) are significant.

5. Case study 1: Proportional-Clegg-Integrator Proportional-Integrator-Derivative (PCI-PID) control system

This section designs a PCI-PID controller on a precision motion stage for validating Theorem 4.

5.1. Precision positioning setup

The plant utilized in this study is a planar motion system with three degrees of freedom as depicted in Fig. 6(a), referred to as "Spyder" stage. This system employs dual leaf flexures, each associated with corresponding masses (M_1, M_2, M_3), for connection to the base (M_c). These masses are driven by three voice coil actuators labeled A_1, A_2, and A_3. Linear encoders (denoted as "Enc"), specifically Mercury M2000 with a resolution of 100 nm and sampled at 10 kHz, are utilized to monitor the positions of the masses. Additionally, with additional oversampling introduced on the FPGA, this resolution is increased to 3.125 nm. For the SISO investigation, only actuator A_1 is used to position mass M_1. The control systems are implemented on an NI compactRIO platform and incorporate a linear current source power amplifier.

Fig. 6(b) depicts the measured Frequency Response Function (FRF) of the system, which exhibits a collocated double mass–spring–damper system with additional high-frequency parasitic dynamics. To improve control clarity, the system is approximated to a single eigenmode mass–spring–damper system using Matlab's identification tool. The transfer function of the system is expressed as:

$$\mathcal{P}(s) = \frac{6.615e5}{83.57s^2 + 279.4s + 5.837e5}. \tag{43}$$

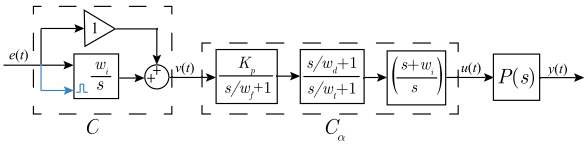

Fig. 7. The open-loop block diagram of the PCI-PID control system.

5.2. The validation and the limitation of Theorem 4 on the analysis of the PCI-PID control system

The PID controller is widely used in industries. Within the PID framework, a PCI-PID controller on the precision motion stage is designed, as shown in Fig. 7. The parameters of the PCI-PID system are as follows: the reset value $\gamma = 0$, $K_p = 20.5$, the cut-off frequency $\omega_c = 2\pi \cdot 150$ [rad/s], $\omega_d = \omega_c/4.8$, $\omega_t = \omega_c \cdot 4.8$, $\omega_f = 10\omega_c$, and $\omega_i = 0.1\omega_c$. The design specifications for the PCI-PID system aim to achieve a crossover frequency of 150 Hz and a phase margin (PM) of 50° in the open-loop. Additionally, the stability and convergence of the system have been verified through testing. Based on simulation observations, in this PCI-PID system under sinusoidal inputs, input frequencies below 37 Hz demonstrate multiple-reset actions, whereas frequencies above 37 Hz exhibit two-reset actions. Note that the frequency range in which multiple-reset systems occur is not limited to low frequencies and can vary depending on the specific reset system structure and design parameters. Further research is needed to develop analytical methods for identifying multiple-reset systems across different configurations.

The steady-state errors indicate the tracking precision of the motion control system. Figs. 8(c_1), (c_2), (d_1), and (d_2) depict the steady-state errors $e(t)$ of the PCI-PID system under input signal $r(t) = 1E{-}7\sin(2\pi f)$ at input frequencies f of 100 Hz and 500 Hz, as predicted, simulated, and measured in experiments. The alignment between the predictions, simulations, and experiments suggests that Theorem 4 accurately predicts the system behavior. Note that the reference input signal used in the experiments is $r(t) = 1E-7\sin(2\pi f t)$ [m].

However, the accuracy of the method in Theorem 4 is limited by Assumption 3. Examples in Fig. 8(a_1), (a_2), (b_1), and (b_2) at input frequencies of 5 Hz and 10 Hz are applied to illustrate this limitation. The jagged noises observed in the experimental signals arise from the sensor's resolution limitations. In these two cases, multiple resets per cycle occur, and Assumption 3 is not satisfied, resulting in inaccuracies in the analysis method. Nevertheless, in practical scenarios, multiple resets may introduce excessive higher-order harmonics to the system, leading to undesired performance issues such as large steady-state error spikes, as shown in Fig. 8(a_1) and (b_1), and limit cycle problems in the PI+CI system (Baños et al., 2011). Therefore, it is preferable to design reset systems without multiple resets across the entire frequency range.

Section 6 introduces a new reset control structure as a case study aimed at addressing the multiple-reset limitation observed in the PCI-PID control structure. This new structure is designed to achieve two reset instants per steady-state cycle, thereby satisfying Assumption 3 required for Theorem 4.

6. Case study 2: Two-reset-PCI-PID (T-PCI-PID) control system

6.1. The two-reset control system

This section introduces a new reset control structure termed the Two-Reset Control System (T-RCS), illustrated in Fig. 9. This structure forces the system to reset twice per steady-state cycle under a single sinusoidal reference input signal, serving as an illustrative example for validating Theorem 4.

In a traditional closed-loop reset system under sinusoidal input $r(t) = |R|\sin(\omega t)$, the error signal $e(t)$ is nonlinear and includes infinitely many harmonics $e_n(t)$ as defined in (13). This new T-RCS introduces a

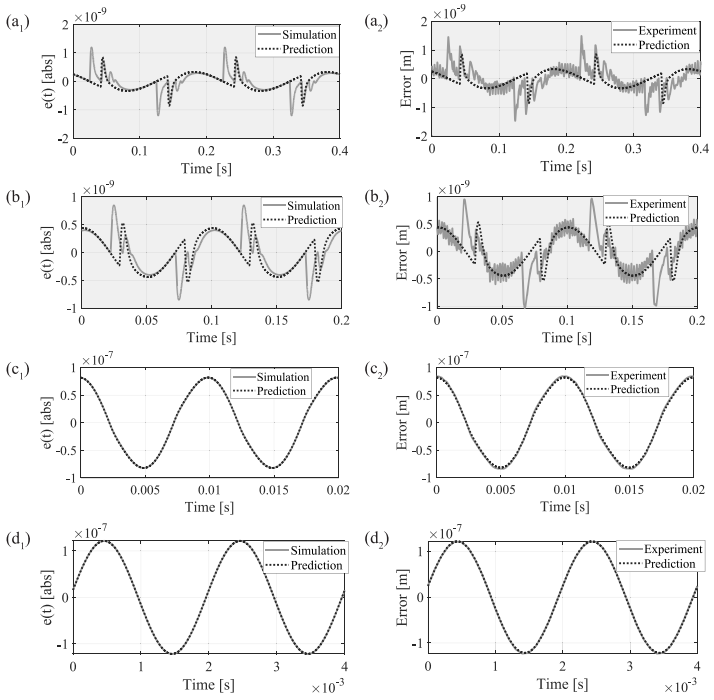

Fig. 8. The steady-state errors $e(t)$ for the PCI-PID system under sinusoidal input $r(t) = \sin(2\pi f t)$ at input frequencies f of 5 Hz in (a_1) and (a_2), 10 Hz in (b_1) and (b_2), 100 Hz in (c_1) and (c_2), and 500 Hz in (d_1) and (d_2) as predicted, simulated, and experimentally measured. The gray background indicates scenarios involving multiple-reset actions.

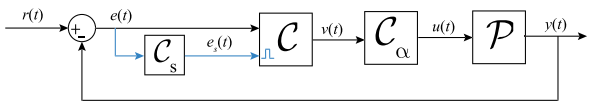

Fig. 9. Block diagram of the T-reset system, where $C_s(s)$ is given in (44) and $e_s(t)$ is the reset signal.

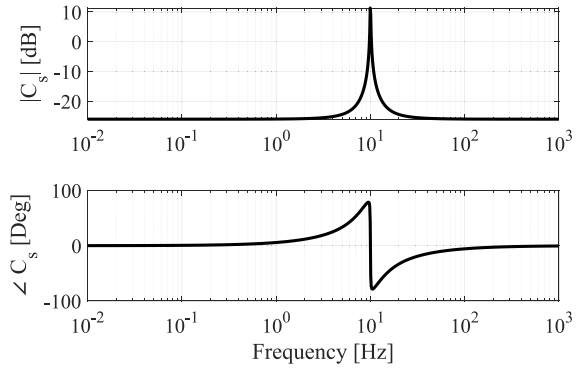

Fig. 10. Bode Plot of $C_s(s)$ for $\omega = 2\pi \cdot 10$ [rad/s].

transfer function C_s between the error signal $e(t)$ and the reset-triggered signal $e_s(t)$. The transfer function of $C_s(s)$ is given by

$$C_s(s) = k_{cs}\left[\frac{(s/(\omega))^2 + s/(\omega \cdot Q_1) + 1}{(s/(\omega))^2 + s/(\omega \cdot Q_2) + 1}\right], \tag{44}$$

where $Q_1 < Q_2 \in \mathbb{R}^+$. In this paper, the parameters are set as $Q_1 = 1$, $Q_2 = 100$, and $k_{cs} = 0.05$.

From (44), $C_s(s)$ functions as an anti-notch filter. This filter allows frequencies within a specific range to pass through while attenuating all others. By adjusting the parameters Q_1 and Q_2, the frequency range of interest can be tailored. For example, selecting $Q_1 = 1$, $Q_2 = 100$, $k_{cs} = 0.05$ for a frequency of $\omega = 2\pi \cdot 10$ [rad/s] yields the Bode plot depicted in Fig. 10. At the frequency $\omega = 2\pi \cdot 10$ [rad/s], $\angle C_s(\omega) = 0$, and the magnitude $|C_s(\omega)|$ is relatively a peak to other frequencies. Therefore, $C_s(s)$ approximately allows signals with a frequency of ω to pass through. By aligning ω with the first-order input frequency in $e(t)$ (13), the reset-triggered signal $e_s(t)$ is approximately expressed as:

$$e_s(t) = |E_1 C_s| \sin(\omega t + \angle E_1). \tag{45}$$

From (45), the reset-triggered signal $e_s(t)$ shares the same frequency and phase as the first-order harmonic $e_1(t)$ in the error signal $e(t)$. Since the reset-triggered signal $e_s(t)$ is phase-dependent and amplitude-independent, Eq. (45) indicates that the reset action of C is triggered based on $e_1(t)$. Thus, within this structure, the T-RCS ensures two reset instants per steady-state. This example serves to validate Theorem 4, satisfying Assumption 3.

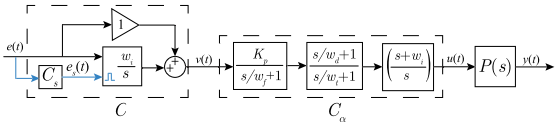

Fig. 11. The open-loop block diagram of the T-PCI-PID control system.

6.2. The application of Theorem 4 to analyze the T-PCI-PID system

6.2.1. The accuracy of Theorem 4

Fig. 11 shows the structure of the Two-reset-PCI PID (T-PCI-PID) Control System. The transfer function C_s is defined in (44). Except for the setting for shaping filter C_s with $Q_1 = 1$, $Q_2 = 100$, $K_{cs} = 0.05$, the parameters of the T-PCI-PID system are specified the same as those of the PCI-PID control system in Case Study 1. It has been verified that the T-PCI-PID system is stable and convergent.

Fig. 12 (a_1)-(d_1) illustrates the simulated and Theorem 4-predicted steady-state errors $e(t)$ for the T-PCI-PID system. In the prediction calculations, 1001 harmonics are included. These simulations consider

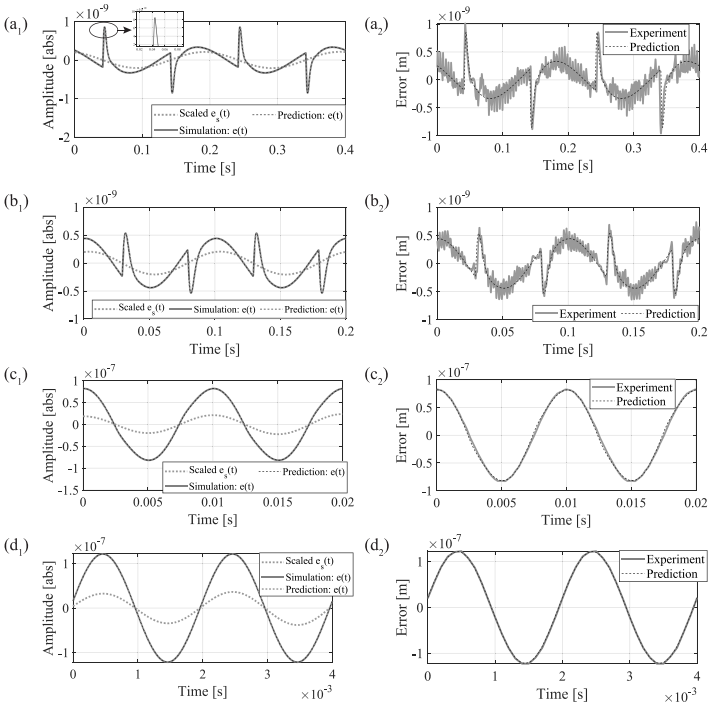

Fig. 12. The steady-state error $e(t)$ for the T-PCI-PID system under sinusoidal input $r(t) = \sin(2\pi f t)$ at input frequencies f of 5 Hz in (a_1) and (a_2), 10 Hz in (b_1) and (b_2), 100 Hz in (c_1) and (c_2), and 500 Hz in (d_1) and (d_2) as predicted, simulated, and experimentally measured. $e_s(t)$ represents the reset triggered signal.

Table 1
The experimentally measured maximum steady-state errors $||e||_\infty$ [m] for PCI-PID and T-PCI-PID control systems at input frequencies of 5 Hz, 10 Hz, 100 Hz, and 500 Hz.

Systems	Frequencies [Hz]			
	5	10	100	500
PCI-PID	1.47E−09	9.57E−10	8.43E−08	1.22E−07
T-PCI-PID	1.01E−09	6.89E−10	8.27E−08	1.22E−07
Error Reduction	31.29%	28.00%	1.90%	0

a reference input signal $r(t) = 1E-7\sin(2\pi f t)$ at frequencies f of 5 Hz, 10 Hz, 100 Hz, and 500 Hz. Given the amplitude-independence of the reset action, the reset-triggered signals are scaled for visual clarity. The reset triggered signal $e_s(t)$ forces two reset instants per steady-state period in multiple-reset systems at input frequencies 5 Hz and 10 Hz, while it maintains the reset instants unchanged in two-reset systems at input frequencies 100 Hz and 500 Hz.

The analytical predictions closely align with the simulations in T-PCI-PID systems, validating the accuracy of Theorem 4. Then, this conclusion is further supported by the experimental results in Fig. 12 (a_2)-(d_2). Note that the jagged signal observed at input frequencies 5 Hz and 10 Hz in the measured results arises from sensor limitations.

Experimental results presented in Fig. 12 not only validate the accuracy of Theorem 4 but also demonstrate the superior performance achieved by the T-PCI-PID system compared to the PCI-PID under sinusoidal inputs. Table 1 compares the maximum steady-state errors $\|e\|_\infty$ for the T-PCI-PID and PCI-PID systems at various input frequencies. Additionally, the table includes the relative error reduction achieved by the T-PCI-PID system compared to the PCI-PID system, highlighting the effectiveness of the proposed design in improving low-frequency precision while preserving high-frequency performance. For example, at an input frequency of 5 Hz, the T-PCI-PID system enhances positioning precision by 31.29%. However, as this paper primarily focuses on developing frequency response analysis for closed-loop reset systems, the broader advantages and limitations of the T-RCS structure in various applications will be examined in future research.

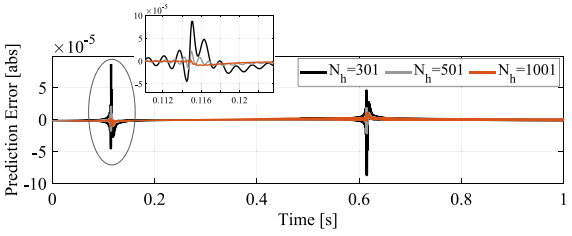

Fig. 13. The PE of the T-PCI-PID control system under the input $r(t) = \sin(2\pi t)$ for different numbers of harmonics (N_h) included in the prediction calculation process, specifically 301, 501, and 1001.

6.2.2. The relation of the accuracy of Theorem 4 and the number of harmonics

Let $e_{\text{sim}}(t)$ and $e_{\text{pre}}(t)$ denote the simulated and predicted steady-state errors in the T-PCI-PID system, respectively. The Prediction Error (PE) between them is defined as $\text{PE} = |e_{\text{sim}}(t) - e_{\text{pre}}(t)|$.

Fig. 13 shows the relationship between the PE and the number of harmonics (denoted as N_h) included in the prediction calculation process, in the T-PCI-PID control system under a sinusoidal input signal $r(t) = \sin(2\pi t)$. As the number of harmonics N_h increases, the accuracy of the method increases. Ideally, PE approaches 0 as N_h tends to infinity. The zoom-in plot emphasizes the differences in predictions between the simulation and Theorem 4, resembling vibration signals. This discrepancy arises because Theorem 4 calculates outputs by summing a finite number of sinusoidal harmonics. The unaccounted infinite harmonics contribute to the prediction error, creating a pattern resembling multi-sine vibrations. Thus, there is a trade-off between the PE and N_h (indicating the calculation time in practice). In practice, readers can strive to minimize PE while considering the computational time trade-off.

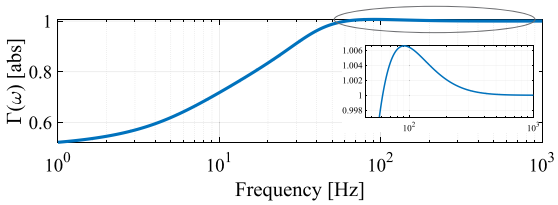

Fig. 14. The $\Gamma(\omega)$ of the T-PCI-PID control system.

6.3. Discussion: The importance of Theorem 4 in the reset systems design

In linear systems, the analytical connection between open-loop and closed-loop frequency-domain analysis serves as an effective tool for designing and predicting the performance of the systems. Let $\mathcal{L}_n(\omega)$ and $\mathcal{S}_n(\omega)$ represent the open-loop transfer function and the closed-loop sensitivity function, respectively. However, in reset systems, the relationship $\mathcal{S}_n(\omega) = 1/(\mathcal{L}_n(\omega) + 1)$ does not hold, neither for the first-order harmonic (for $n = 1$) nor higher-order harmonics (for $n > 1$). The developed closed-loop sensitivity functions in (38) illustrate that the first and higher-order harmonics in the open-loop have a cross effect on the first and higher-order harmonics in the closed-loop, mediated by the parameter $\Gamma(\omega)$.

As highlighted in Remark 4, Method A and Method B assume $\Gamma(\omega) = 1$ for all ω, which implies that higher-order harmonics $e_n(t)$ for $n > 1$ undergo no reset actions, leading to inaccuracies. Theorem 4 addresses this issue by introducing the parameter $\Gamma(\omega)$. The parameter $\Gamma(\omega)$ affects computations for both first-order and higher-order harmonics, as demonstrated in Eqs. (38) to (41). Its introduction provides a more accurate representation of the system's behavior, particularly in scenarios involving significant higher-order harmonics. Moreover, $\Gamma(\omega)$ can be used to design and tune reset systems to be less affected by higher-order harmonics, for improving system performance.

Fig. 14 illustrates the $\Gamma(\omega)$ values in the T-PCI-PID system when subjected to sinusoidal inputs across frequencies ranging from 1 Hz to 1000 Hz. It is evident from the figure that $\Gamma(\omega) = 1$ does not hold across the entire frequency range. Given this context, comparing the new method with previous Methods A and B would be redundant, as these methods have already been shown to make inaccurate assumptions. To validate the accuracy of the new theorem, its predictions are directly compared with simulation and experimental results in Section 6.2.1. Note that the depiction of $\Gamma(\omega)$ in Fig. 14 specifically pertains to the system described in case study 2. For different reset control systems, $\Gamma(\omega)$ will vary as determined by (37).

As discussed in Remark 2, $\Gamma(\omega)$ provides a measure of the relative magnitude of higher-order harmonics $\sum_{n=3}^{\infty} v_{nl}^{n}(t)$ compared to the first-order harmonic $v_{nl}^{1}(t)$. This metric can be utilized in future system designs to adjust system parameters and mitigate the relative effects of higher-order harmonics in closed-loop systems, while retaining the first-order harmonic performance.

6.4. Discussion: Future work of Applying Theorems 1–4 in the Reset Systems Design

For the steady-state performance analysis of closed-loop reset systems, as discussed in the last subsection, relying solely on open-loop analysis is inadequate due to the influence of higher-order harmonics. The sensitivity function $\mathcal{S}_n(\omega)$ in Theorem 4 serves as a critical closed-loop indicator of steady-state error across different frequencies.

For instance, Fig. 15 illustrates the sensitivity function derived from Theorem 4 for the closed-loop T-PCI-PID system. A low magnitude of $|\mathcal{S}_n(\omega)|$ signifies high accuracy in the system's steady-state response. This metric can guide the tuning of reset systems to achieve enhanced positioning accuracy at targeted frequencies.

Moreover, research (Karbasizadeh et al., 2022) demonstrated that higher-order harmonics in closed-loop reset systems are tunable. However, the underlying theoretical principles for the closed-loop harmonics remain unclear. Ideally, the goal is to maintain the benefits of first-order harmonics while minimizing higher-order harmonics to negligible levels. Achieving this would allow the superposition law hold for closed-loop reset systems under multiple inputs. The open-loop and closed-loop analysis presented in Theorems 1 through 4 provide effective tools for such tuning and designing of reset control systems.

For transient-state performance analysis, the peak of the sensitivity function $\mathcal{S}_n(\omega)$, denoted as M_s, serves as an indicator. For instance, in linear systems, a high M_s value at frequencies corresponding to significant disturbances or errors often correlates with higher overshoot (Shamsuzzoha & Skogestad, 2010). When the magnitudes of higher-order harmonics are relatively much lower compared to the first-order harmonics at frequencies where the sensitivity function peaks, this linear relationship can be approximately extended to closed-loop reset systems.

For illustration, three PCI-PID reset systems with different design parameters are presented. The design parameters of System 1 are detailed in Section 5.2. System 2 is configured with the following parameters: reset value $\gamma = 0$, $K_p = 13.9$, $\omega_c = 2\pi \cdot 140$ rad/s, $\omega_d = \omega_c/6.1$, $\omega_t = \omega_c \cdot 6.1$, $\omega_f = 10\omega_c$, and $\omega_i = 0.1\omega_c$. System 3 is designed with the following parameters: reset value $\gamma = 0$, $K_p = 28.5$, $\omega_c = 2\pi \cdot 160$ rad/s, $\omega_d = \omega_c/3.9$, $\omega_t = \omega_c \cdot 3.9$, $\omega_f = 10\omega_c$, and $\omega_i = 0.1\omega_c$.

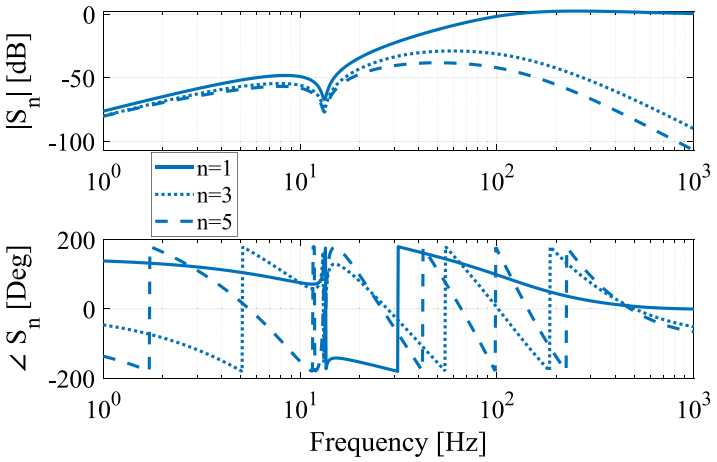

Fig. 15. The Bode plot of the closed-loop Higher Order Sinusoidal Input Sensitivity Function (HOSISF) $\mathcal{S}_n(\omega)$ for the closed-loop T-PCI-PID control system, with the first three harmonics S_1, S_3, and S_5.

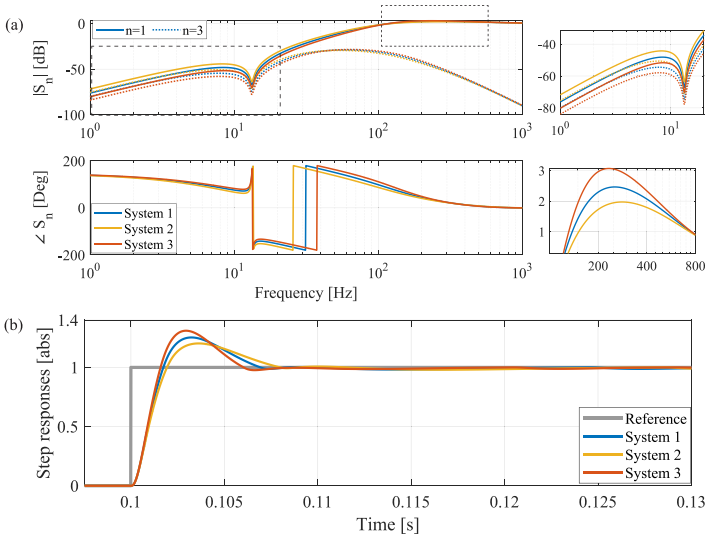

Fig. 16. (a) The $S_n(\omega)$ with the first and third harmonics S_1 and S_3 for three closed-loop PCI-PID control system. (b) The step responses of these three systems by simulation.

Fig. 16(a) illustrates the sensitivity functions of three reset systems. For clarity, only the two primary harmonics — the first-order ($n = 1$) and third-order ($n = 3$) harmonics — are displayed. Among these three systems, System 2 exhibits the lowest peak sensitivity function (M_s). Additionally, at the frequencies where M_s peaks, the magnitudes of higher-order harmonics are relatively low and therefore negligible, satisfying the two-reset assumptions of Theorem 4. The step response comparison among the three systems presented in Fig. 16(b) further reveals that System 2 has the lowest overshoot. These findings suggest that when higher-order harmonics can be omitted, higher M_s values in the first-order harmonics are associated with larger overshoot in the closed-loop system, consistent with observations in linear systems. Therefore, maintaining M_s below a specified threshold helps prevent excessive overshoot and reduces sensitivity to inputs. However, this analysis provides only a preliminary evaluation of frequency-domain characteristics and transient response. A more rigorous investigation into the relationship between transient response behavior and the sensitivity function $S_n(\omega)$ is crucial for a deeper understanding and optimization of reset control systems. Additionally, the step response analysis for closed-loop reset systems detailed in Zhang and HosseinNia (2024) serves as a tool for conducting the transient response analysis.

In summary, developing designing and tuning guideline to optimize both steady-state and transient responses in reset systems is crucial for their industrial application. The contributions in this work, including Theorems 1 to 4, provide foundational frequency-domain tools for this purpose.

7. Conclusion

To conclude, this study develops frequency response analysis methods for open-loop and closed-loop reset control systems with two reset actions per steady-state cycle. These methods establish connections between the open-loop and closed-loop analysis of reset systems. Simulation and experimental results on a precision motion stage validate the accuracy and efficacy of the proposed methods. Moreover, the results highlight the potential application of these methods to facilitate future reset control system design in the frequency domain.

However, the proposed frequency response analysis is currently limited to two-reset systems. In practical design, it is preferable to avoid multiple-reset systems since they introduce high-magnitude higher-order harmonics, which may degrade performance. Nonetheless, in scenarios where multiple-reset actions are unavoidable, future research will be necessary to develop accurate analysis methods tailored to these systems.

Additionally, the frequency response analysis for closed-loop reset systems under sinusoidal disturbance and noise inputs follows a similar derivation process to the theorems presented in this paper. To maintain clarity on the contribution of this work, this analysis is not included here but will be addressed in future research.

Furthermore, the newly introduced Two-Reset Control System (T-RCS) is designed to ensure two-reset systems, which serves as an illustrative example validating the main contribution of this work. Notably, the T-RCS has demonstrated improved steady-state tracking precision at low frequencies compared to traditional reset systems when subjected to sinusoidal reference inputs. This enhanced performance can be attributed to the elimination of multiple-reset occurrences achieved by the T-RCS. Future research will comprehensively explore the practical application of the T-RCS under various types of inputs.

CRediT authorship contribution statement

Xinxin Zhang: Writing – original draft, Writing – review & editing, Visualization, Validation, Software, Resources, Project administration, Methodology, Investigation, Formal analysis, Data curation, Conceptualization. **Marcin B. Kaczmarek:** Writing – review, Discussion. **S. Hassan HosseinNia:** Writing – review & editing, Supervision, Resources, Project administration, Methodology, Investigation, Conceptualization.

Declaration of competing interest

The authors declare that they have no known competing financial interests or personal relationships that could have appeared to influence the work reported in this paper.

Declaration of Generative AI and AI-assisted technologies in the writing process

During the preparation of this work the authors used [ChatGPT] in order to improve readability and language. After using this tool, the authors reviewed and edited the content as needed and take full responsibility for the content of the publication.

Acknowledgement

Xinxin Zhang acknowledges the PhD grant from the China Scholarship Council.

Appendix A. Proof for Lemma 1

Proof. Consider a GCI (with $A_R = 0, B_R = 1, C_R = 1, D_R = 0$) subjected to a sinusoidal input signal $e(t) = |E_1|\sin(\omega t)$, under Assumption 1 and the Zeno-free condition in (10), at steady states.

Based on (1), the output signal $u_{ci}(t)$ of the GCI is given by

$$\begin{cases} \dot{u}_{ci}(t) = e(t), & e(t) \neq 0, \\ u_{ci}(t^+) = \gamma u_{ci}(t), & e(t) = 0. \end{cases} \tag{A.1}$$

For its BLS (which is an integrator), we have

$$\dot{u}_i(t) = e(t). \tag{A.2}$$

Define $q_i(t) = u_{ci}(t) - u_i(t)$. From (A.1) and (A.2), we have

$$\begin{cases} \dot{q}_i(t) = \dot{u}_{ci}(t) - \dot{u}_i(t) = 0, & e(t) \neq 0, \\ q_i(t^+) = \gamma q_i(t) + (\gamma - 1)u_i(t), & e(t) = 0. \end{cases} \tag{A.3}$$

The reset instant of the GCI with a sinusoidal input signal $e(t) = |E_1|\sin(\omega t)$ is determined by $t_i = i\pi/\omega$, where $i \in \mathbb{Z}^+$ and $e(t_i) = 0$. Utilizing (A.3), the signal $q_i(t)$ between two consecutive reset instants $[t_i^+, t_{i+1}]$ (where t_i^+ denotes the after-reset instant) is expressed as:

$$q_i(t) = q_i(t_i^+) + \int_{t_i}^{t} \dot{q}_i(\tau)d\tau = q_i(t_i^+), \ t \in [t_i^+, t_{i+1}]. \tag{A.4}$$

Given the input signal $e(t) = |E_1|\sin(\omega t)$ and based on the state-space equation in (1), at the reset instant $t_i = i\pi/\omega$, the base-linear output $u_i(t_i)$ is given by:

$$u_i(t_i) = \begin{cases} 0, & \text{for even } i, \\ 2|E_1|/\omega, & \text{for odd } i. \end{cases} \tag{A.5}$$

Combining (A.3), (A.4), and (A.5), at the reset instant t_i, $q_i(t_i^+)$ is given by

$$\begin{aligned} q_i(t_i^+) &= \gamma q_i(t_{i-1}^+) + (\gamma - 1)u_i(t_i) \\ &= \begin{cases} \gamma q_i(t_{i-1}^+), & \text{for even } i, \\ \gamma q_i(t_{i-1}^+) + 2|E_1|(\gamma - 1)/\omega, & \text{for odd } i. \end{cases} \end{aligned} \tag{A.6}$$

Based on (A.6), for an odd i, $q_i(t_i^+)$ is given by

$$\begin{aligned} q_i(t_i^+) &= q_i(t_{i+2}^+) \\ &= \gamma q_i(t_{i+1}^+) + 2|E_1|(\gamma - 1)/\omega \\ &= \gamma^2 q_i(t_i^+) + 2|E_1|(\gamma - 1)/\omega. \end{aligned} \tag{A.7}$$

Eqs. (A.6) and (A.7) can be concluded that

$$q_i(t_i^+) = \begin{cases} -2|E_1|\gamma(\gamma + 1)^{-1}/\omega, & \text{for even } i, \\ -2|E_1|(\gamma + 1)^{-1}/\omega, & \text{for odd } i. \end{cases} \tag{A.8}$$

Combining (A.4) and (A.8), $q_i(t)$ in the time domain can be derived as follows:

$$q_i(t) = \begin{cases} -2|E_1|\gamma(\gamma + 1)^{-1}/\omega, & \text{for } t \in [2k, 2k + 1) \cdot \pi/\omega, \\ -2|E_1|(\gamma + 1)^{-1}/\omega, & \text{for } t \in [2k + 1, 2k + 2) \cdot \pi/\omega. \end{cases} \tag{A.9}$$

Here we conclude the proof. □

Appendix B. Proof for Theorem 1

Proof. Consider a reset controller $\mathcal{C}$ (1) where $n_r = 1$ with an input signal of $e(t) = |E_n|\sin(n\omega t + \angle E_n)$ ($\angle E_s \in (-\pi, \pi)$, $n = 2k + 1$, $k \in \mathbb{N}$) and a reset triggered signal of $e_s(t) = |E_s|\sin(\omega t + \angle E_s)$ ($\angle E_s \in (-\pi, \pi)$), at steady states. Let $x_c(t)$ and $x_{bl}(t)$ denote the state and the base-linear state of the $\mathcal{C}$ and the BLC $\mathcal{C}_{bl}$, respectively. Define

$$x_{nl}(t) = x_c(t) - x_{bl}(t) \ (\in \mathbb{R}^{n_c \times 1}), \tag{B.1}$$

where n_c is the number of states of the reset controller $\mathcal{C}$ and $x_{bl}(t)$ is given by

$$x_{bl}(t) = |E_n \Delta_l(n\omega)|\sin(n\omega t + \angle E_n + \angle \Delta_l(n\omega)), \tag{B.2}$$

where

$$\Delta_l(n\omega) = (jn\omega I - A_R)^{-1} B_R \ (\in \mathbb{R}^{n_c \times 1}). \tag{B.3}$$

Based on (1) and (B.1), we have:

$$\begin{cases} \dot{x}_{nl}(t) = A_R x_{nl}(t), & e_s(t) \neq 0, \\ x_{nl}(t^+) = A_\rho x_{nl}(t) + (A_\rho - I)x_{bl}(t), & e_s(t) = 0. \end{cases} \tag{B.4}$$

For the reset controller $\mathcal{C}$ with a reset triggered signal of $e_s(t) = |E_s|\sin(\omega t + \angle E_s)$, the set of reset instants is denoted by $J_o := \{t_i \mid t_i = (i\pi - \angle E_s)/\omega, \ i \in \mathbb{Z}^+\}$. The reset interval is given by $\sigma_i = t_{i+1} - t_i = \pi/\omega$. According to (B.4), between two consecutive reset instants $[t_i^+, t_{i+1}]$ where $e_s(t) \neq 0$, the expression for $x_{nl}(t)$ is given by

$$x_{nl}(t) = e^{A_R(t - t_i)}\Delta_n(\omega), \quad \text{for } t \in [t_i^+, t_{i+1}], \tag{B.5}$$

where $\Delta_n(\omega) \in \mathbb{R}^{n_c \times 1}$ is a constant matrix independent of time t.

Based on (B.5), at the reset instant $t_{i+1} \in J_o$, $x_{nl}(t_{i+1})$ is given by

$$x_{nl}(t_{i+1}) = e^{A_R(t_{i+1} - t_i)}\Delta_n(\omega) = e^{A_R\pi/\omega}\Delta_n(\omega). \tag{B.6}$$

From (B.4), $x_{nl}(t^+)$ at the reset instant t_{i+1} is given by

$$x_{nl}(t_{i+1}^+) = A_\rho x_{nl}(t_{i+1}) + (A_\rho - I)x_{bl}(t_{i+1}). \tag{B.7}$$

Substituting $x_{nl}(t_{i+1})$ from (B.6) into (B.7), $x_{nl}(t_{i+1}^+)$ is obtained as

$$x_{nl}(t_{i+1}^+) = A_\rho e^{A_R\pi/\omega}\Delta_n(\omega) + (A_\rho - I)x_{bl}(t_{i+1}). \tag{B.8}$$

From (B.2), at the reset instant $t_i = (i\pi - \angle E_s)/\omega$, the base-linear state is given by

$$\begin{aligned} x_{bl}(t_i) &= |E_n \Delta_l(n\omega)|\sin(ni\pi + \angle E_n + \angle \Delta_l(n\omega) - n\angle E_s) \\ &= \begin{cases} |E_n \Delta_l(n\omega)|\sin(\angle \Delta_l(n\omega) + \angle E_n - n\angle E_s), & \text{for even } i, \\ -|E_n \Delta_l(n\omega)|\sin(\angle \Delta_l(n\omega) + \angle E_n - n\angle E_s), & \text{for odd } i, \end{cases} \end{aligned} \tag{B.9}$$

where $\Delta_l(n\omega)$ is given in (B.3).

Define

$$\Delta_c^n(\omega) = |\Delta_l(n\omega)|\sin(\angle \Delta_l(n\omega) + \angle E_n - n\angle E_s) \ (\in \mathbb{R}^{n_c \times 1}), \tag{B.10}$$

and substitute $\Delta_c^n(\omega)$ from (B.10) into (B.9), we have

$$x_{bl}(t_i) = \begin{cases} |E_n|\Delta_c^n(\omega), & \text{for even } i, \\ -|E_n|\Delta_c^n(\omega), & \text{for odd } i. \end{cases} \tag{B.11}$$

From (B.11), at the reset instant $t_{i+1} = ((i+1)\pi - \angle E_s)/\omega$, the expression for $x_{bl}(t_{i+1})$ is written as:

$$x_{bl}(t_{i+1}) = \begin{cases} -|E_n|\Delta_c^n(\omega), & \text{for even } i, \\ |E_n|\Delta_c^n(\omega), & \text{for odd } i, \end{cases} \tag{B.12}$$

Substituting $x_{bl}(t_{i+1})$ from (B.12) into (B.8), $x_{nl}(t_{i+1}^+)$ is derived as

$$x_{nl}(t_{i+1}^+) = \begin{cases} A_\rho e^{A_R\pi/\omega}\Delta_n(\omega) - (A_\rho - I)|E_n|\Delta_c^n(\omega), & \text{for even } i, \\ A_\rho e^{A_R\pi/\omega}\Delta_n(\omega) + (A_\rho - I)|E_n|\Delta_c^n(\omega), & \text{for odd } i. \end{cases} \tag{B.13}$$

From (B.13), we have

$$x_{nl}(t_i^+) = \begin{cases} A_\rho e^{A_R\pi/\omega}\Delta_n(\omega) + (A_\rho - I)|E_n|\Delta_c^n(\omega), & \text{for even } i, \\ A_\rho e^{A_R\pi/\omega}\Delta_n(\omega) - (A_\rho - I)|E_n|\Delta_c^n(\omega), & \text{for odd } i. \end{cases} \tag{B.14}$$

From (B.5), at the reset instant t_i^+, we have

$$x_{nl}(t_i^+) = \Delta_n(\omega). \tag{B.15}$$

Let Eqs. (B.14) and (B.15) be set equal to each other. Then, $\Delta_n(\omega)$ is derived as follows:

$$\Delta_n(\omega) = \begin{cases} |E_n|\Delta_v^n(\omega), & \text{for even } i, \\ -|E_n|\Delta_v^n(\omega), & \text{for odd } i, \end{cases} \tag{B.16}$$

where

$$\Delta_v^n(\omega) = (A_\rho e^{A_R\pi/\omega} - I)^{-1}(I - A_\rho)\Delta_c^n(\omega)\ (\in \mathbb{R}^{n_c\times 1}). \tag{B.17}$$

Since the reset interval $\sigma_i = \pi/\omega$, Eqs. (B.5) and (B.16) together illustrate that $x_{nl}(t)$ is bounded and has the same period $2\pi/\omega$ as the reset triggered signal $e_s(t)$. The absolute integrability of $x_{nl}(t)$ implies the existence of its Fourier and Laplace transforms. Let $X_{nl}(s)$ denote the Laplace transform of $x_{nl}(t)$. From (B.5), for $t \in [t_i^+,\ t_{i+1}]$, the Laplace transform of $x_{nl}(t)$ is expressed as:

$$X_{nl}(s) = \mathscr{L}[x_{nl}(t)] = (sI - A_R)^{-1}e^{-A_R t_i}\Delta_n(\omega). \tag{B.18}$$

Define a parameter $Q(s) = \mathscr{L}[q(t)]$ as:

$$Q(s) = (sI)^{-1}(sI - A_R)X_{nl}(s). \tag{B.19}$$

Then, based on (B.18) and (B.19), for $t \in [t_i^+,\ t_{i+1}]$, $Q(s)$ is given by

$$Q(s) = (sI)^{-1}e^{-A_R t_i}\Delta_n(\omega). \tag{B.20}$$

From (B.16) and (B.20), during the time interval $[t_i^+,\ t_{i+1}]$, the inverse Laplace transform of $Q(s)$ is given by:

$$q(t) = \mathscr{L}^{-1}[Q(s)] = \begin{cases} |E_n|\Delta_v^n(\omega)u(t - t_i) + C_{\beta 1}, & \text{for even } i, \\ -|E_n|\Delta_v^n(\omega)u(t - t_i) + C_{\beta 2}, & \text{for odd } i, \end{cases} \tag{B.21}$$

where $u(t)$ is an unit step signal. The parameters $C_{\beta 1} \in \mathbb{R}^{n_c\times 1}$ and $C_{\beta 2} \in \mathbb{R}^{n_c\times 1}$ are the values of $q(t)$ at the reset instant t_i. From (B.21), we obtain that $q(t)$ remains a constant matrix during the time interval $[t_i^+,\ t_{i+1}]$.

From (B.5), at the time instant t_{i+1}, $x_{nl}(t_{i+1}) = e^{A_R\pi/\omega}\Delta_n(\omega)$. From (B.16), $x_{nl}(t_i)$ is given by

$$x_{nl}(t_i) = \begin{cases} -|E_n|e^{A_R\pi/\omega}\Delta_v^n(\omega), & \text{for even } i, \\ |E_n|e^{A_R\pi/\omega}\Delta_v^n(\omega), & \text{for odd } i, \end{cases} \tag{B.22}$$

From (B.5) and (B.16), at the time instant t_i^+, $x_{nl}(t_i^+)$ is given by

$$x_{nl}(t_i^+) = \begin{cases} |E_n|\Delta_v^n(\omega), & \text{for even } i, \\ -|E_n|\Delta_v^n(\omega), & \text{for odd } i. \end{cases} \tag{B.23}$$

From the time instant t_i to t_i^+, $x_{nl}(t_i)$ jumps to $x_{nl}(t_i^+)$. From (B.22) and (B.23), this jump is given by

$$x_{nl}(t_i^+) - x_{nl}(t_i) = \begin{cases} |E_n|(I + e^{A_R\pi/\omega})\Delta_v^n(\omega), & \text{for even } i, \\ -|E_n|(I + e^{A_R\pi/\omega})\Delta_v^n(\omega), & \text{for odd } i. \end{cases} \tag{B.24}$$

Substituting $\Delta_v^n(\omega)$ from (B.17) into (B.24), we have

$$x_{nl}(t_i^+) - x_{nl}(t_i) = \begin{cases} |E_n|(I + e^{A_R\pi/\omega})(A_\rho e^{A_R\pi/\omega} - I)^{-1}(I - A_\rho)\Delta_c^n(\omega), & \text{for even } i, \\ -|E_n|(I + e^{A_R\pi/\omega})(A_\rho e^{A_R\pi/\omega} - I)^{-1}(I - A_\rho)\Delta_c^n(\omega), & \text{for odd } i. \end{cases} \tag{B.25}$$

Define

$$\Delta_q^n(\omega) = (I + e^{A_R\pi/\omega})(A_\rho e^{A_R\pi/\omega} - I)^{-1}(I - A_\rho)\Delta_c^n(\omega)\ (\in \mathbb{R}^{n_c\times 1}) \tag{B.26}$$

and substitute $\Delta_q^n(\omega)$ from (B.26) into (B.25), we have

$$x_{nl}(t_i^+) - x_{nl}(t_i) = \begin{cases} |E_n|\Delta_q^n(\omega), & \text{for even } i, \\ -|E_n|\Delta_q^n(\omega), & \text{for odd } i. \end{cases} \tag{B.27}$$

This jump indicates that from the time instant t_i to t_i^+, $x_{nl}(t)$ is an impulse signal denoted by $\zeta_{nl}(t)$. From (B.27), $\zeta_{nl}(t)$ is expressed as:

$$\zeta_{nl}(t) = [x_{nl}(t_i^+) - x_{nl}(t_i)]\delta(t - t_i) = \begin{cases} |E_n|\Delta_q^n(\omega)\delta(t - t_i), & \text{for even } i, \\ -|E_n|\Delta_q^n(\omega)\delta(t - t_i), & \text{for odd } i, \end{cases} \tag{B.28}$$

where $\delta(t)$ represents the Dirac delta function.

Since the Laplace transform of the delta function is 1, the Laplace transform of the impulse signal $\zeta_{nl}(t)$ in (B.28) is given by:

$$\zeta_{nl}(s) = \begin{cases} |E_n|\Delta_q^n(\omega)e^{-t_i s}, & \text{for even } i, \\ -|E_n|\Delta_q^n(\omega)e^{-t_i s}, & \text{for odd } i. \end{cases} \tag{B.29}$$

The impulse response is defined as the response of a system to a Dirac delta input (Pesaran & Shin, 1998). Define a signal $\zeta_q(t)$ as the impulse response of the impulse signal $\zeta_{nl}(t)$ filtered through the linear time invariant (LTI) transfer function $(sI)^{-1}(sI - A_R)$. From (B.29), $\zeta_q(t)$ is given by:

$$\zeta_q(t) = \mathscr{L}^{-1}[(sI)^{-1}(sI - A_R)\zeta_{nl}(s)] = \begin{cases} |E_n|\Delta_q^n(\omega)\delta(t - t_i) - |E_n|A_R\Delta_q^n(\omega), & \text{for even } i, \\ -|E_n|\Delta_q^n(\omega)\delta(t - t_i) + |E_n|A_R\Delta_q^n(\omega), & \text{for odd } i. \end{cases} \tag{B.30}$$

Eq. (B.30) demonstrates that at the time instant t_i, $\zeta_q(t_i)$ has an initial value of $\pm|E_n|A_R\Delta_q^n(\omega)$ and undergoes a jump of:

$$\zeta_q(t_i^+) - \zeta_q(t_i) = \begin{cases} |E_n|\Delta_q^n(\omega), & \text{for even } i, \\ -|E_n|\Delta_q^n(\omega), & \text{for odd } i. \end{cases} \tag{B.31}$$

From (B.19), the signal $x_{nl}(t)$ filtered by $(sI)^{-1}(sI - A_R)$ generates the signal $q(t)$. Eqs. (B.30) and (B.31) demonstrate that at the time instant t_i to t_i^+, the signal $x_{nl}(t_i)$ jumps to $x_{nl}(t_i^+)$. The jump $\zeta_{nl}(t)$, filtered by the transfer function $(sI)^{-1}(sI - A_R)$, generates a jump $\zeta_q(t_i^+) - \zeta_q(t_i)$ in (B.31). Thus, from (B.19), (B.30), and (B.31), the jump in $q(t) = \mathscr{L}^{-1}[Q(s)]$ at the time instant t_i is given by:

$$q(t_i^+) - q(t_i) = \zeta_q(t_i^+) - \zeta_q(t_i). \tag{B.32}$$

Based on (B.31) and (B.32), at the time instant t_i, we have

$$q(t_i^+) = \begin{cases} q(t_i) + |E_n|\Delta_q^n(\omega), & \text{for even } i, \\ q(t_i) - |E_n|\Delta_q^n(\omega), & \text{for odd } i. \end{cases} \tag{B.33}$$

From (B.21), $q(t_i^+)$ for even i is given by

$$q(t_i^+) = |E_n|\Delta_v^n(\omega) + C_{\beta 1}. \tag{B.34}$$

From (B.33), at the time instant t_i for even i, $q(t_i^+) = q(t_i) + |E_n|\Delta_q^n(\omega)$. Then, based on (B.21) and (B.33), $q(t_i^+)$ for even i can be written as

$$q(t_i^+) = -|E_n|\Delta_v^n(\omega) + C_{\beta 2} + |E_n|\Delta_q^n(\omega). \tag{B.35}$$

By setting Eqs. (B.34) and (B.35) equal to each other, we get:

$$C_{\beta 1} = C_{\beta 2} - 2|E_n|\Delta_v^n(\omega) + |E_n|\Delta_q^n(\omega). \tag{B.36}$$

Substituting $C_{\beta 1}$ from (B.36) to (B.21), $q(t)$ is given by

$$q(t) = \begin{cases} -|E_n|\Delta_v^n(\omega)u(t - t_{2k}) + |E_n|\Delta_q^n(\omega) + C_{\beta 2}, & \text{for } t \in [t_{2k}^+,\ t_{2k+1}], \\ -|E_n|\Delta_v^n(\omega)u(t - t_{2k+1}) + C_{\beta 2}, & \text{for } t \in [t_{2k+1}^+,\ t_{2k+2}], \end{cases} \tag{B.37}$$

where $k \in \mathbb{N}$.

Let $f(t)_k$ ($k \in \mathbb{Z}^+$) represent the kth state of a function $f(t)$. Considering the reset controller $\mathcal{C}$ (1) with resetting the first state where $n_r = 1$, the first state $x_c(t_i)_1$ in the state $x_c(t_i)$ is reset to $\gamma x_c(t_i)_1$, and there are no reset actions in state $x_c(t)_k$ for $k > 1$. Therefore, we have

$$x_c(t)_k = x_{bl}(t)_k, \text{ for } k > 1. \tag{B.38}$$

From (B.1), (B.28), and (B.38), we have

$$\begin{aligned} &x_{nl}(t)_k = 0, \text{ for } k > 1, \\ &\Delta_q^n(\omega)_k = 0, \text{ for } k > 1. \end{aligned} \tag{B.39}$$

From (B.19) and (B.39), we have

$$q(t)_k = 0, \text{ for } k > 1. \tag{B.40}$$

Eq. (B.37) indicates that during the time interval $[t_i^+,\ t_{i+1}]$, $q(t)$ is a constant matrix. Eq. (B.33) demonstrates that at the time instant $t_i \in J_o$, $q(t)$ has a jump of $\pm|E_n|\Delta_q^n(\omega)$. Therefore, the signal $q(t)$ is absolutely integrable, ensuring the existence of its Fourier and Laplace transforms. Since $\sigma_i = t_{i+1} - t_i = \pi/\omega$, from (B.33), (B.37), and (B.40), the first state of $q(t)$ denoted by $q(t)_1$ is a square wave with a period of $2\pi/\omega$. It shares the same phase as the reset triggered signal $e_s(t)$ and has a magnitude of $|E_n|\Delta_q^n(\omega)_1$. Define a normalized square wave signal $q_s(t)$ with the same phase as the reset-triggered signal $e_s(t)$, expressed as follows:

$$q_s(t) = \frac{4}{\pi}\sum_{\mu=1}^{\infty}\frac{\sin(\mu\omega t + \mu\angle E_s)}{\mu},\ \mu = 2k+1 (k \in \mathbb{N}), \tag{B.41}$$

whose Fourier transform is given by

$$Q_s(\omega) = \mathcal{F}[q_s(t)] = 4\sum_{\mu=1}^{\infty}\mathcal{F}[\sin(\mu\omega t + \mu\angle E_s)]/(\mu\pi). \tag{B.42}$$

According to (B.37), (B.40) and (B.41), $q(t)$ can be expressed as:

$$q(t) = |E_n|\Delta_q^n(\omega)q_s(t)/2 - |E_n|\Delta_v^n(\omega) + C_{\beta 2} + |E_n|\Delta_q^n(\omega)/2. \tag{B.43}$$

For a time-domain signal $q(t)$, the frequency ω is a constant. A constant function corresponds to a delta function in the frequency domain. Defining $Q(\omega) = \mathcal{F}[q(t)]$, we derive $Q(\omega)$ from (B.43) as follows:

$$Q(\omega) = |E_n|\Delta_q^n(\omega)Q_s(\omega)/2 + (|E_n|\Delta_q^n(\omega)/2 - \Delta_v^n(\omega) + C_{\beta 2})\delta(\omega). \tag{B.44}$$

Since $\delta(\omega)$ is a Dirac delta function, which is zero for $\omega \neq 0$, Eq. (B.44) is simplified as:

$$Q(\omega) = |E_n|\Delta_q^n(\omega)Q_s(\omega)/2. \tag{B.45}$$

From (B.42) and (B.45), $Q(\omega)$ is given by

$$Q(\omega) = 2|E_n|\Delta_q^n(\omega)\sum_{\mu=1}^{\infty}\mathcal{F}[\sin(\mu\omega t + \mu\angle E_s)]/(\mu\pi). \tag{B.46}$$

Both $Q(\omega)$ (B.46) and $Q_s(\omega)$ (B.42) contain μ harmonics. Let $Q^\mu(\omega)$ and $Q_s^\mu(\omega)$ represent the μ-th ($\mu \in \mathbb{Z}^+$) harmonics of $Q(\omega)$ and $Q_s(\omega)$, respectively. They are expressed as:

$$\begin{aligned} Q(\omega) &= \sum_{\mu=1}^{\infty} Q^\mu(\omega), \\ Q_s(\omega) &= \sum_{\mu=1}^{\infty} Q_s^\mu(\omega). \end{aligned} \tag{B.47}$$

From (B.42), (B.46), and (B.47), $Q_s^\mu(\omega)$ and $Q^\mu(\omega)$ are given by

$$\begin{aligned} Q_s^\mu(\omega) &= 4\mathcal{F}[\sin(\mu\omega t + \mu\angle E_s)]/(\mu\pi), \\ Q^\mu(\omega) &= 2|E_n|\Delta_q^n(\omega)\mathcal{F}[\sin(\mu\omega t + \mu\angle E_s)]/(\mu\pi). \end{aligned} \tag{B.48}$$

Let $X_{nl}(\omega) = \mathcal{F}[x_{nl}(t)]$, and $X_{nl}^\mu(\omega)$ represents the μ-th harmonic of $X_{nl}^\mu(\omega)$, defined as:

$$X_{nl}(\omega) = \sum_{\mu=1}^{\infty} X_{nl}^\mu(\omega). \tag{B.49}$$

From (B.19), (B.48) and (B.49), $X_{nl}^\mu(\omega)$ is derived as

$$X_{nl}^\mu(\omega) = (j\mu\omega I - A_R)^{-1} j\mu\omega I Q^\mu(\omega). \tag{B.50}$$

According to (B.1), (B.49), and (B.50), $X_c(\omega) = \mathcal{F}[x_c(t)]$ is obtained as

$$X_c(\omega) = X_{bl}(\omega) + \sum_{\mu=1}^{\infty}(j\mu\omega I - A_R)^{-1} j\mu\omega I Q^\mu(\omega), \tag{B.51}$$

where $X_{bl}(\omega) = \mathcal{F}[x_{bl}(t)]$.

Let $V(\omega) = \mathcal{F}[v(t)]$. According to (1), $V(\omega)$ is given by

$$V(\omega) = C_R X_c(\omega) + D_R E(\omega). \tag{B.52}$$

Substituting $X_c(\omega)$ from (B.51) into (B.52), $V(\omega)$ is given by

$$V(\omega) = C_R X_{bl}(\omega) + D_R E(\omega) + \sum_{\mu=1}^{\infty} C_R(j\mu\omega I - A_R)^{-1} j\mu\omega I Q^\mu(\omega). \tag{B.53}$$

From (1), we have

$$V_{bl}(\omega) = C_{bl}(\omega)E(\omega) = C_R X_{bl}(\omega) + D_R E(\omega). \tag{B.54}$$

Then, substituting $V_{bl}(\omega)$ from (B.54) into (B.53), $V(\omega)$ is given by

$$V(\omega) = V_{bl}(\omega) + \sum_{\mu=1}^{\infty} C_R(j\mu\omega I - A_R)^{-1} j\mu\omega I Q^\mu(\omega). \tag{B.55}$$

Define

$$\begin{aligned} V_{nl}(\omega) &= \sum_{\mu=1}^{\infty} V_q^\mu(\omega), \\ V_q^\mu(\omega) &= \Delta_x(\mu\omega)Q^\mu(\omega), \\ \Delta_x(\mu\omega) &= C_R(j\mu\omega I - A_R)^{-1} j\mu\omega I\ (\in \mathbb{R}^{1\times n_c}). \end{aligned} \tag{B.56}$$

and substitute $V_q^\mu(\omega)$ from (B.56) into (B.55), $V(\omega)$ is then given by

$$V(\omega) = V_{bl}(\omega) + V_{nl}(\omega) = V_{bl}(\omega) + \sum_{\mu=1}^{\infty} V_q^\mu(\omega). \tag{B.57}$$

In the time domain, Eq. (B.57) is given by

$$v(t) = v_{bl}(t) + v_{nl}(t). \tag{B.58}$$

From (B.56), $v_{nl}(t)$ is given by

$$v_{nl}(t) = \mathcal{F}^{-1}\left[\sum_{\mu=1}^{\infty}\Delta_x(\mu\omega)Q^\mu(\omega)\right],\ \mu \in \mathbb{Z}^+, \tag{B.59}$$

where $Q^\mu(\omega)$ and $\Delta_x(\mu\omega)$ are defined in (B.56) and (B.48), respectively. Eqs. (B.58) and (B.59) conclude the proof. □

Appendix C. Proof for Theorem 2

Proof. The reset controller C, operating with the input signal and reset-triggered signal $e(t) = |E_1|\sin(\omega t + \angle E_1)$ at steady states is defined as the reset controller discussed in Theorem 1 when $e_s(t) = e(t)$.

Following a similar proof process as in Appendix B, consider that there are $n \in \mathbb{N}$ harmonics in the reset output signal $v(t)$. Referring to (B.57), let $V(\omega) = \sum_{n=1}^{\infty} V_n(\omega)$, we obtain $V_n(\omega)$ as

$$V_n(\omega) = \begin{cases} V_{bl}(\omega) + V_q^1(\omega), & \text{for } n = 1, \\ V_q^n(\omega), & \text{for odd } n > 1, \\ 0, & \text{for even } n \geq 2. \end{cases} \tag{C.1}$$

By applying the "Virtual Harmonic Generator" (Saikumar et al., 2021), the input signal $e(t)$ generates n harmonics $e_{1n}(t) = |E_1|\sin(n\omega t + n\angle E_1)$, whose Fourier transform is $E_{1n}(\omega) = |E_1|\mathcal{F}[\sin(n\omega t + n\angle E_1)]$. From (B.56), $C_{nl}(n\omega)$ is defined as

$$C_{nl}(n\omega) = \frac{V_q^n(\omega)}{E_{1n}(\omega)} = 2\Delta_x(n\omega)\Delta_q(\omega)/(n\pi). \tag{C.2}$$

From (B.54), (C.1), and (C.2), the nth HOSIDF for C, denoted as $C_n(\omega)$, is defined as

$$C_n(\omega) = \frac{V_n(\omega)}{E_{1n}(\omega)} = \begin{cases} C_{bl}(\omega) + C_{nl}(\omega), & \text{for } n = 1, \\ C_{nl}(n\omega), & \text{for odd } n > 1, \\ 0, & \text{for even } n \geq 2. \end{cases} \tag{C.3}$$

This concludes the proof. □

Appendix D. Proof for Corollary 1

Proof. Define

$$V_{nl}(\omega) = \sum_{n=1}^{\infty} V_q^n(\omega). \tag{D.1}$$

From (C.2), we have

$$V_q^n(\omega) = E_{1n}(\omega)C_{nl}(n\omega). \tag{D.2}$$

From (D.1) and (D.2), the inverse Fourier transform of $V_{nl}(\omega)$ is given by

$$v_{nl}(t) = \sum_{n=1}^{\infty} \mathcal{F}^{-1}[E_{1n}(\omega)C_{nl}(n\omega)]. \tag{D.3}$$

From (B.57) and (D.1), $V(\omega)$ given by

$$V(\omega) = V_{bl}(\omega) + V_{nl}(\omega). \tag{D.4}$$

The inverse Fourier transform of $V(\omega)$ is given in (25). This concludes the proof. □

Appendix E. Proof for Theorem 3

Proof. Consider a closed-loop reset control system (with reset controller C (1) where $n_r = 1$), as depicted in Fig. 1 with a sinusoidal reference input signal $r(t) = |R|\sin(\omega t)$ and under Assumptions 2 and 3, at steady states.

The Fourier transform of (32) is given by

$$\begin{aligned} V_l(\omega) &= \sum_{n=1}^{\infty} V_{bl}^n(\omega), \\ V_{nl}(\omega) &= \sum_{n=1}^{\infty} V_{nl}^n(\omega). \end{aligned} \tag{E.1}$$

Based on (35) and (E.1), the signal $v_l(t)$ in (33) is given by

$$v_l(t) = \sum_{n=1}^{\infty} \mathcal{F}^{-1}[E_n(\omega)C_{bl}(n\omega)]. \tag{E.2}$$

The following section outlines the derivation of the signal $v_{nl}(t)$ in (33). This process commences with the derivation of its first-order harmonic $v_{nl}^1(t)$. According to (25), the first C under an input signal and the reset-triggered signal of $e_1(t) = |E_1|\sin(\omega t + \angle E_1)$, yields the base-linear output denoted by $v_{bl}^1(t)$ and the nonlinear output signal denoted by $v_{nl}^1(t)$. To generate the signal $v_{nl}^1(t)$, the "Virtual Harmonic Generator" is employed to generate harmonics $e_{1n}(t)$ from $e_1(t)$, as illustrated in Fig. 5(a), as given by:

$$e_{1n}(t) = |E_1|\sin(n\omega t + n\angle E_1), \ \ n = 2k + 1 (k \in \mathbb{N}), \tag{E.3}$$

whose Fourier transform is $E_{1n}(\omega) = \mathcal{F}[e_{1n}(t)]$.

The signal $v_{bl}^1(t)$ is derived by (35). From (C.2), the signal $v_{nl}^1(t)$ is given by:

$$v_{nl}^1(t) = \sum_{n=1}^{\infty} \mathcal{F}^{-1}[E_{1n}(\omega)C_{nl}(n\omega)]. \tag{E.4}$$

In Fig. 5(a), consider a reset controller C with a sinusoidal input signal $e_n(t) = |E_n|\sin(n\omega t + \angle E_n)$ and a reset triggered signal $e_1(t) = |E_1|\sin(\omega t + \angle E_1)$. From (34), $V^n(\omega)$ is given by

$$V^n(\omega) = V_{bl}^n(\omega) + V_{nl}^n(\omega). \tag{E.5}$$

From (21), $V_{nl}^n(\omega)$ is given by

$$V_{nl}^n(\omega) = \sum_{\mu=1}^{\infty} \Delta_x(\mu\omega)Q^{\mu}(\omega), \tag{E.6}$$

where $\Delta_x(\mu\omega)$ and $Q^{\mu}(\omega)$ are given in (22).

From (E.6), $V_{nl}^n(\omega)$, for a constant ω and varying n, exhibit the same phase as the reset-triggered signal $e_1(t)$. Considering that $V_{nl}^n(\omega)$ exhibits the same phase for different n, as indicated in (E.1), we introduce a function $\Gamma(\omega)$ to express the ratio of $V_{nl}(\omega)$ to $V_{nl}^1(\omega)$:

$$\Gamma(\omega) = \frac{V_{nl}(\omega)}{V_{nl}^1(\omega)} = \frac{\sum_{n=1}^{\infty} V_{nl}^n(\omega)}{V_{nl}^1(\omega)}. \tag{E.7}$$

From (E.4) and (E.7), $V_{nl}(\omega)$ is given by

$$V_{nl}(\omega) = \sum_{n=1}^{\infty} \Gamma(\omega)E_{1n}(\omega)C_{nl}(n\omega). \tag{E.8}$$

From (E.1) and (E.8), we have

$$V_{nl}^n(\omega) = \Gamma(\omega)E_{1n}(\omega)C_{nl}(n\omega). \tag{E.9}$$

Eqs. (33), (E.2), and (E.8) describe the new block diagram for the closed-loop RCS, presented in Fig. 5(b). In the new block diagram, the unknown parameter $\Gamma(\omega)$ will be elucidated in the subsequent derivation.

By substituting $V_{nl}^n(\omega)$ from (22) and (E.6) into (E.7), $\Gamma(\omega)$ is simplified as

$$\Gamma(\omega) = \frac{\sum_{n=1}^{\infty} |E_n|\Delta_c^n(\omega)}{|E_1|\Delta_c^1(\omega)}. \tag{E.10}$$

As illustrated in Fig. 5(b), in the closed-loop configuration, we have

$$E_n(\omega) = -V_n(\omega)C_{\alpha}(n\omega)\mathcal{P}(n\omega). \tag{E.11}$$

Substituting (35) and (E.9) into (34), $V_n(\omega)$ is given by

$$V_n(\omega) = E_n(\omega)C_{bl}(n\omega) + \Gamma(\omega)E_{1n}(\omega)C_{nl}(n\omega). \tag{E.12}$$

Substituting (E.12) into (E.11), we have

$$E_n(\omega) = -E_n(\omega)\mathcal{L}_{bl}(n\omega) - \Gamma(\omega)E_{1n}(\omega)\mathcal{L}_{nl}(n\omega), \tag{E.13}$$

where

$$\begin{aligned} \mathcal{L}_{bl}(n\omega) &= C_{bl}(n\omega)C_{\alpha}(n\omega)\mathcal{P}(n\omega), \\ \mathcal{L}_{nl}(n\omega) &= C_{nl}(n\omega)C_{\alpha}(n\omega)\mathcal{P}(n\omega). \end{aligned} \tag{E.14}$$

Based on the definitions of $e_n(t)$ and $e_{1n}(t)$ provided in (13) and (E.3), we express (E.13) in the time domain as follows:

$$|E_n \parallel 1+\mathcal{L}_{bl}(n\omega)|\sin(n\omega t+\angle E_n+\angle(1+\mathcal{L}_{bl}(n\omega)))= -\Gamma(\omega)|E_1 \parallel \mathcal{L}_{nl}(n\omega)|\sin(n\omega t+n\angle E_1+\angle\mathcal{L}_{nl}(n\omega)). \tag{E.15}$$

From (E.15) and the given condition $|E_n|>0$, we can deduce the following equations:

$$|E_n|=\frac{\Gamma(\omega)|\mathcal{L}_{nl}(n\omega)|}{|1+\mathcal{L}_{bl}(n\omega)|}|E_1|,\ \text{for } n=2k+1>1,\ \text{and}$$
$$\angle E_n=n\pi+n\angle E_1+\angle\mathcal{L}_{nl}(n\omega)-\angle(1+\mathcal{L}_{bl}(n\omega)),\ \text{for } n=2k+1>1. \tag{E.16}$$

From (22), $\Delta_c^n(\omega)$ is given by

$$\Delta_c^n(\omega)=|\Delta_l(n\omega)|\sin(\angle\Delta_l(n\omega)+\angle E_n-n\angle E_1). \tag{E.17}$$

Substituting the relation between $\angle E_1$ and $\angle E_n(n>1)$ from (E.16) into (E.17), we obtain:

1. For $n=1$,
$$\Delta_c^1(\omega)=|\Delta_l(\omega)|\sin(\angle\Delta_l(\omega)). \tag{E.18}$$
2. For $n>1$,
$$\Delta_c^n(\omega)=-|\Delta_l(n\omega)|\sin(\angle\Delta_l(n\omega)+\angle\mathcal{L}_{nl}(n\omega)-\angle(1+\mathcal{L}_{bl}(n\omega))). \tag{E.19}$$

Then, substituting $\Delta_c^n(\omega)$ from (E.18) and (E.19) into (E.10), we have

$$\Gamma(\omega)=1+\frac{\sum_{n=3}^{\infty}|E_n|\Delta_c^n(\omega)}{|E_1|\Delta_c^1(\omega)}. \tag{E.20}$$

Define

$$\Psi_n(\omega)=|\mathcal{L}_{nl}(n\omega)|/|1+\mathcal{L}_{bl}(n\omega)| \tag{E.21}$$

and substitute $\Psi_n(\omega)$ from (E.21) into (E.16), we then obtain:

$$|E_n|=\Gamma(\omega)\Psi_n(\omega)|E_1|,\ \text{for } n>1. \tag{E.22}$$

Substituting (E.21) and (E.22) into (E.20), $\Gamma(\omega)$ is given by

$$\Gamma(\omega)=1+\Gamma(\omega)\frac{\sum_{n=3}^{\infty}\Psi_n(\omega)\Delta_c^n(\omega)}{\Delta_c^1(\omega)}. \tag{E.23}$$

Derived from (E.23), $\Gamma(\omega)$ is obtained as below:

$$\Gamma(\omega)=1/\left(1-\sum_{n=3}^{\infty}\Psi_n(\omega)\Delta_c^n(\omega)/\Delta_c^1(\omega)\right). \tag{E.24}$$

Here, $\Gamma(\omega)$ is derived and the proof of Theorem 3 is concluded. □

Appendix F. Proof for Theorem 4

Proof. Consider a closed-loop SISO reset control system in Fig. 1 with a reset controller C (1) (where $n_r=1$) and to a sinusoidal reference input signal $r(t)=|R|\sin(\omega t)$, complying with Assumptions 2 and 3, at steady states.

From the block diagram for the closed-loop reset system in Fig. 5(b), we can express the first harmonic of the output $Y(\omega)$ as $Y_1(\omega)$, given by

$$Y_1(\omega)=E_1(\omega)[\mathcal{L}_{bl}(\omega)+\Gamma(\omega)\mathcal{L}_{nl}(\omega)], \tag{F.1}$$

where $\mathcal{L}_{bl}(n\omega)$ and $\mathcal{L}_{nl}(n\omega)$ are given in (E.14).

Let $R_n(\omega)=|R|\mathcal{F}[\sin(n\omega t)]$, in the closed loop, we have

$$Y_1(\omega)=R_1(\omega)-E_1(\omega). \tag{F.2}$$

Combining (F.1) and (F.2), the first order sensitivity function for the closed-loop reset system, denoted as $S_1(\omega)$ is given by

$$S_1(\omega)=\frac{E_1(\omega)}{R(\omega)}=\frac{1}{1+\mathcal{L}_{bl}(\omega)+\Gamma(\omega)\mathcal{L}_{nl}(\omega)}. \tag{F.3}$$

Define

$$\mathcal{L}_o(n\omega)=\mathcal{L}_{bl}(n\omega)+\Gamma(\omega)\mathcal{L}_{nl}(n\omega). \tag{F.4}$$

Substituting (F.4) into (F.3), $S_1(\omega)$ is given by

$$S_1(\omega)=\frac{1}{1+\mathcal{L}_o(\omega)}. \tag{F.5}$$

From (E.3) and (F.3), we obtain

$$E_{1n}(\omega)=|S_1(\omega)|e^{jn\angle S_1(\omega)}R_n(\omega), \tag{F.6}$$

where $R_n(\omega)=|R|\mathcal{F}[\sin(n\omega t)]$.

Combining (E.13) and (F.6), the nth (for $n=2k+1>1,\ k\in\mathbb{N}$) order sensitivity function for the closed-loop reset system, denoted by $S_n(\omega)$ is given by

$$S_n(\omega)=\frac{E_n(\omega)}{R_n(\omega)}=\frac{-\Gamma(\omega)\mathcal{L}_{nl}(n\omega)}{1+\mathcal{L}_{bl}(n\omega)}\frac{E_{1n}(\omega)}{R_n(\omega)}=-\frac{\Gamma(\omega)\mathcal{L}_{nl}(n\omega)|S_1(\omega)|e^{jn\angle S_1(\omega)}}{1+\mathcal{L}_{bl}(n\omega)}. \tag{F.7}$$

According to Theorems 2 and 3, the even harmonics of $S_n(\omega)$ are zeros. The nth order complementary sensitivity function $\mathcal{T}_n(\omega)$ in (39) and the control sensitivity function $\mathcal{CS}_n(\omega)$ in (40) can be derived using the same method from (F.1) to (F.7). This concludes the proof. □

References

Banos, A., & Barreiro, A. (2012). *Reset control systems*. Springer.

Baños, A., Dormido, S., & Barreiro, A. (2011). Limit cycles analysis of reset control systems with reset band. *Nonlinear Analysis: Hybrid Systems*, *5*(2), 163–173.

Baños, A., & Vidal, A. (2007). Definition and tuning of a PI+ CI reset controller. In *2007 European control conference* (pp. 4792–4798). IEEE.

Barabanov, E., & Konyukh, A. (2001). Bohl exponents of linear differential systems. *Memoirs on Differential Equations and Mathematical Physics*, *24*, 151–158.

Barreiro, A., Baños, A., Dormido, S., & González-Prieto, J. A. (2014). Reset control systems with reset band: Well-posedness, limit cycles and stability analysis. *Systems & Control Letters*, *63*, 1–11.

Beerens, R., Bisoffi, A., Zaccarian, L., Nijmeijer, H., Heemels, M., & van de Wouw, N. (2021). Reset PID design for motion systems with stribeck friction. *IEEE Transactions on Control Systems Technology*, *30*(1), 294–310.

Beker, O. (2001). *Analysis of reset control systems*. University of Massachusetts Amherst.

Beker, O., Hollot, C., Chait, Y., & Han, H. (2004). Fundamental properties of reset control systems. *Automatica*, *40*(6), 905–915.

Carrasco, J., Baños, A., & Barreiro, A. (2008). Stability of reset control systems with inputs. In *2008 16th Mediterranean conference on control and automation* (pp. 1496–1501). IEEE.

Chen, L., Saikumar, N., Baldi, S., & HosseinNia, S. H. (2018). Beyond the waterbed effect: Development of fractional order crone control with non-linear reset. In *2018 annual American control conference* (pp. 545–552). IEEE.

Clegg, J. C. (1958). A nonlinear integrator for servomechanisms. *Transactions of the American Institute of Electrical Engineers, Part II: Applications and Industry*, *77*(1), 41–42.

Dastjerdi, A. A., Astolfi, A., Saikumar, N., Karbasizadeh, N., Valerio, D., & HosseinNia, S. H. (2022). Closed-loop frequency analysis of reset control systems. *IEEE Transactions on Automatic Control*, *68*(2), 1146–1153.

Deenen, D., Heertjes, M. F., Heemels, W., & Nijmeijer, H. (2017). Hybrid integrator design for enhanced tracking in motion control. In *2017 American control conference* (pp. 2863–2868). IEEE.

Deenen, D. A., Sharif, B., van den Eijnden, S., Nijmeijer, H., Heemels, M., & Heertjes, M. (2021). Projection-based integrators for improved motion control: Formalization, well-posedness and stability of hybrid integrator-gain systems. *Automatica*, *133*, Article 109830.

Guo, Y., & Chen, Y. (2019). Stability analysis of delayed reset systems with distributed state resetting. *Nonlinear Analysis. Hybrid Systems*, *31*, 265–274.

Guo, Y., Wang, Y., & Xie, L. (2009). Frequency-domain properties of reset systems with application in hard-disk-drive systems. *IEEE Transactions on Control Systems Technology*, *17*(6), 1446–1453.

Hazeleger, L., Heertjes, M., & Nijmeijer, H. (2016). Second-order reset elements for stage control design. In *2016 American control conference* (pp. 2643–2648). IEEE.

Heertjes, M., Gruntjens, K., Van Loon, S., Van de Wouw, N., & Heemels, W. (2016). Experimental evaluation of reset control for improved stage performance. *IFAC-PapersOnLine*, *49*(13), 93–98.

Heinen, K. (2018). Frequency analysis of reset systems containing a clegg integrator: An introduction to higher order sinusoidal input describing functions.

Horowitz, I., & Rosenbaum, P. (1975). Non-linear design for cost of feedback reduction in systems with large parameter uncertainty. *International Journal of Control*, *21*(6), 977–1001.

Kaczmarek, M. B., Zhang, X., & HosseinNia, S. H. (2022). Steady-state nonlinearity of open-loop reset systems. In *2022 IEEE conference on control technology and applications* (pp. 1056–1060). IEEE.

Karbasizadeh, N., Dastjerdi, A. A., Saikumar, N., & HosseinNia, S. H. (2022). Band-passing nonlinearity in reset elements. *IEEE Transactions on Control Systems Technology*, *31*(1), 333–343.

Karbasizadeh, N., & HosseinNia, S. H. (2022). Continuous reset element: Transient and steady-state analysis for precision motion systems. *Control Engineering Practice*, *126*, Article 105232.

Karbasizadeh, N., Saikumar, N., & HosseinNia, S. H. (2021). Fractional-order single state reset element. *Nonlinear Dynamics*, *104*, 413–427.

Krishnan, K., & Horowitz, I. (1974). Synthesis of a non-linear feedback system with significant plant-ignorance for prescribed system tolerances. *International Journal of Control*, *19*(4), 689–706.

Nuij, P., Bosgra, O., & Steinbuch, M. (2006). Higher-order sinusoidal input describing functions for the analysis of non-linear systems with harmonic responses. *Mechanical Systems and Signal Processing*, *20*(8), 1883–1904.

Ogata, K. (2010). *Modern control engineering*. Upper Saddle River, NJ: Prentice Hall.

Pavlov, A., van de Wouw, N., & Nijmeijer, H. (2007). Frequency response functions for nonlinear convergent systems. *IEEE Transactions on Automatic Control*, *52*(6), 1159–1165.

Pavlov, A., Van De Wouw, N., & Nijmeijer, H. (2006). *Uniform output regulation of nonlinear systems: A convergent dynamics approach*: *vol. 205*, Springer.

Pesaran, H. H., & Shin, Y. (1998). Generalized impulse response analysis in linear multivariate models. *Economics Letters*, *58*(1), 17–29.

Saikumar, N., Heinen, K., & HosseinNia, S. H. (2021). Loop-shaping for reset control systems: A higher-order sinusoidal-input describing functions approach. *Control Engineering Practice*, *111*, Article 104808.

Saikumar, N., & HosseinNia, H. (2017). Generalized fractional order reset element (GFrORE). In *9th European nonlinear dynamics conference*. EUROMECH.

Saikumar, N., Sinha, R. K., & HosseinNia, S. H. (2019). "Constant in gain lead in phase" element–application in precision motion control. *IEEE/ASME Transactions on Mechatronics*, *24*(3), 1176–1185.

Samad, T., Mastellone, S., Goupil, P., van Delft, A., Serbezov, A., & Brooks, K. (2019). Ifac industry committee update, initiative to increase industrial participation in the control community. Newsletters April 2019. IFAC.

Shamsuzzoha, M., & Skogestad, S. (2010). The setpoint overshoot method: A simple and fast closed-loop approach for PID tuning. *Journal of Process Control*, *20*(10), 1220–1234.

Tian, G., & Gao, Z. (2007). Frequency response analysis of active disturbance rejection based control system. In *2007 IEEE international conference on control applications* (pp. 1595–1599). IEEE.

Van Loon, S., Gruntjens, K., Heertjes, M. F., van de Wouw, N., & Heemels, W. (2017). Frequency-domain tools for stability analysis of reset control systems. *Automatica*, *82*, 101–108.

Wang, T., Sun, J., Wang, X., Liu, Y., Si, Y., Dong, J. S., Yang, X., & Li, X. (2014). A systematic study on explicit-state non-Zenoness checking for timed automata. *IEEE Transactions on Software Engineering*, *41*(1), 3–18.

Weise, C., Wulff, K., & Reger, J. (2019). Fractional-order memory reset control for integer-order LTI systems. In *2019 IEEE 58th conference on decision and control* (pp. 5710–5715). IEEE.

Weise, C., Wulff, K., & Reger, J. (2020). Extended fractional-order memory reset control for integer-order LTI systems and experimental demonstration. *IFAC-PapersOnLine*, *53*(2), 7683–7690.

Zhang, X., & HosseinNia, S. H. (2024). Transient response analysis of reset PID control systems. In *4th IFAC conference on advances in proportional-integral-derivative control - Almeria, Spain*.

Zhao, G., Hua, C., & Guan, X. (2020). Reset observer-based zeno-free dynamic event-triggered control approach to consensus of multiagent systems with disturbances. *IEEE Transactions on Cybernetics*, *52*(4), 2329–2339.

Zhao, G., Nešić, D., Tan, Y., & Hua, C. (2019). Overcoming overshoot performance limitations of linear systems with reset control. *Automatica*, *101*, 27–35.

Zhao, G., & Wang, J. (2015). Existence and design of non-overshoot reset controllers for minimum-phase linear single-input single-output systems. *IET Control Theory & Applications*, *9*(17), 2514–2521.

Zhao, G., & Wang, J. (2016). On L2 gain performance improvement of linear systems with Lyapunov-based reset control. *Nonlinear Analysis. Hybrid Systems*, *21*, 105–117.